Modelling Reflexed-Based Crawling Over Curved Terrain

A thesis submitted by

Robert D. Kaufman

In partial fulfillment of the requirements for the degree of

Master of Science

in

Mechanical Engineering

Tufts University

Advisor: Professor Jason Rife

Submitted: August 2017

Abstract

Soft-bodied robotics represents an exciting new frontier with the potential to enable tasks that humans can't do due to space, environmental, or safety limitations. Much work has been done towards mimicking biological systems in the control and design of crawling soft-bodied robots. A numerical model is proposed that adapts analysis conducted previously by Schuldt *et al*. to a wider variety of terrain, and in particular to crawling on non-planar substrates. Matlab Simulation results show the model crawls just as robustly in non-planar environments as in the planar ones investigated in prior work.

Acknowledgements

First and foremost, I'd like to thank my parents, Wendy and Jeff, for their immeasurable contributions, material, emotional, and genetic, that have brought me to this point. Quite literally, this wouldn't have been possible without them. I'd also like to thank my brothers, Alex and Max, for their support, even if it was more often implicit than explicit. To my better half, Leah, thank you for being there for me when I needed it throughout this process, and for being so accommodating of the time demands. Credit is also due to my best friend and longest non-familial cohabitant, Chris Jackson, for his support as well as for reviewing one of the final drafts of this thesis (along with my brother Alex and roommate Phil Deardorff).

Thanks Obama. I say so unironically.

I am eternally appreciative of everything Tufts University has doe for me as I have made it my home (in varying levels) since arriving here in September of 2009. I am also deeply grateful to the numerous faculty members of Tufts University Department of Mechanical Engineering who have so greatly influenced my academic development. I would also like to thank the unsung heroes of the Tufts Operations Division, who keep our campus running day in and day out, and the men and women of the Tufts University Police Department and Department of Pubic Safety for ensuring a safe environment for learning, teaching, and research.

I owe a special thanks to my committee members, Professor Gary Leisk and Professor Bruce Panilaitis. Beyond Professor Leisk's role as my academic advisor, it was his lecture, in a seminar class taught by Professor Panilaitis, that initially sparked my interest in soft-bodied robotics. A year and a half later, we've come full circle. I am also indebted to Dieter Schuldt for

his comprehensive and innovative work upon which mine expands. To quote Sir Isaac Newton, "If I have seen further, it is by standing on the shoulders of giants."

And last, but certainly not least, is my thesis advisor, Professor Jason Rife. Beyond his role guiding me through this process, which would be beyond noteworthy in and of itself, he has played a role in every step of my education here at Tufts, dating back to the first day I stepped on campus in August 2008 (see Figure A). In addition to his current role, he has served as my teacher (during both my undergraduate and graduate education), research advisor (allowing me to explore more in the controls space the summer while I was still plotting my next steps the summer after my senior year), Academic Dean (despite me not officially being his charge), commencement name reader (when he did me a solid and recognized the handwritten "cum laude" stamp on my marching card because I didn't have a chance to get the official one), ad-hoc admissions counselor (again, see figure A), quasi-therapist (as graduate studies almost always require), and mentor. Jason, thank you.

Robert Kaufman <robertdkaufman@gmail.com> 8/24/08

to jason.rife

Dear Dr. Rife,

I just wanted to thank you once again for taking the time to sit down with my mother and me on Friday. I really enjoyed our conversation and am very excited by all that Tufts and Tufts Engineering have to offer. I was very impressed by my visit to Tufts and do think that Tufts would be a great fit for me.

Sincerely,
Robert

Figure A. My first-ever e-mail correspondence with Prof. Rife in response to meeting him during my first-ever visit to Tufts the summer before my senior year of high school.

Table of Contents

List of Figures

List of Tables

1. Introduction

A. Motivation

It is in uncontrolled environments that the next big gains from robotic innovation will come. Robots can be used to perform operations in areas that are inhospitable to human activity, which could occur due to the presence of hazardous materials, threat of violence from animals or hostile groups, possibility of collapse or explosion, etc. Further, there is the possibility to use them in environments too small for humans to enter, such as confined spaces caused by man-made or natural catastrophes, industrial machinery, smaller sections of structures, and even inside the human body for diagnostics or treatments.[1] The challenge becomes accomplishing these varied tasks with minimal energy use but maximum structural flexibility as well as navigational and locomotive capabilities.

Soft-bodied robotics represents an exciting new avenue for accomplishing many of these goals. Soft bodies offer a number of advantages over conventional materials, such as rigid metals and plastics. These include higher capabilities in confined spaces (particularly those that vary in size and shape, such as a collapsed building), as well as better safety when interacting with biological systems (such as performing diagnostic imaging on a human patient).[2] While almost all tissue in the body is soft, medical instruments are, for the most part, hard. This lack of compatibility can lead to injuries. One such example is bowel perforations caused by the introduction of a rigid endoscope into the soft bowel tissue.[2] There are also applications for soft-body robotics within medical rehabilitation through the use of wearable

robots.[3] While the need for and benefit of soft-body robotics is well-demonstrated, there is still much work to be done to make their wide-spread use a reality.

B. Prior Work

The research required to make soft-body robotics possible addresses a number of inter-related challenges. Some of these challenges include design, fabrication, sensing, control, navigation, actuation, and locomotion. To meet these challenges, much effort has been focused on developing soft-body robots that mimic real-life animals. Recent work has included the development of soft-body robotic systems inspired by organisms such as octopuses, jellyfish, snakes, and caterpillars, among others.[1]

Locomotion in soft-bodied robots presents a number of challenges, the majority stem from the decreased (or altogether absent) ability of soft materials to transmit forces in the way hard materials do. The proposed techniques to achieve soft-bodied locomotion are varied. Worm-like actuation has been achieved through use of dielectric elastomers[1,4] and shape-memory actuators.[1,5] Other work has focused on mimicking the octopus' unique ability to vary the stiffness of its arms while remaining pliable.[1,6,7] Fish-like robots have been developed utilizing fluidic actuators.[1,8] Rolling[1,9, 10] and quadrupedal[1,11] motion have also been examined. Onal and Rus utilized four bidirectional fluidic elastomer actuators to power a snake-like robot through a retrograde (fore to aft) curvature wave.[1,12] Other work has focused on ideas as novel as combustion to power soft-robot locomotion.[13]

Caterpillars have been identified as an interesting model for soft-body robots due to their ability to travel over varied and difficult terrain. This terrain includes confined spaces, compliant surfaces, and vertical and inverted terrain.[14] Further, caterpillar gait is kinematically

consistent, whether the caterpillar is crawling on horizontal or vertical terrain.[15] This ability exists throughout numerous stages of caterpillar development, even when they undergo significant growth (sometimes as much as 10,000 fold).[16,17,13] This locomotion occurs despite the lack of a coordinated central nervous system or rigid skeleton (prior work has shown that caterpillars transmit forces through the substrate, forming a so-called "environmental skeleton").[18]

Locomotion is achieved through the use of grippers known as crochets (referencing Figure 1, the crochets are visible on the side of the caterpillar attached to the leaf). A caterpillar's crochets are located on each of their main body segments, known as abdominal prolegs (these segments are visible in figure 1, but will be discussed in greater detail in Chapter 2A).[13,19] These crochets passively attach to any surface with which they come into contact. This contributes to a caterpillar's ability to traverse vertical and inverted surfaces with very little energy use.[13,20] Thus, developing a caterpillar-like soft-bodied robot is contingent on developing a robust method for controlling its crochets. Schuldt et. al adapted a model[21,22] for simulating intersegment dynamics of a snake in order to examine how a caterpillar's gait could be mimicked with a reflex-based, local-sensing control model (although there are some key differences between a snake and a caterpillar, namely the lack of crochets).[13] Their model, which will be describe in detail in chapter 2a, represents a caterpillar-like soft-bodied robot as a series of masses linked by springs, dampers, and muscles which crawls through the use of muscles and grippers. Their work demonstrated that such a model could provide for robust locomotion on a flat or inclined plane.

C. Knowledge Gap

Schuldt's work provides a novel template on which to model a soft-bodied caterpillar-like robot. Further, he demonstrated that such a template could provide for a regular and repeatable gait over a wide range of system parameters. However, his work stopped short of demonstrating crawling capabilities over non-planar terrain. The notion that the earth, particularly the ecosystems in which caterpillars live, is non-planar is fairly intuitive (see Figures 1 and 2). And while some man-made environments (such as a building) may have more uniform planar environments, the fact remains that, even in man-made environments, a robot will have to transition between planar zones. Two hypothetical environments where a soft-bodied robot might need to operate include an urban search and rescue environment (Figure 3) and a human colon (Figure 4).

Figure 1 Caterpillar crawling on leaf (source:www.absfreepic.com under Creative Commons 0 License)[23]

Figure 2 Caterpillar transitioning from one branch segment to another (source:www.absfreepic.com under Creative Commons 0 License)[24]

Figure 3 Exterior view of 9/11 rubble showing angulated, irregular debris (source: National Archives and Records Administration)[25]

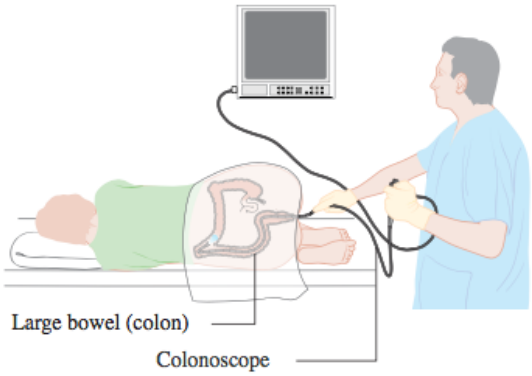

Figure 4 Colonoscopy procedure showing the geometry challenges involved (source:commons.wikimedia.org under Creative Commons By Standard Attribution License) [26]

D. Contributions

The challenge then becomes how to adapt Schuldt's model for travel in non-planar environments. There are theoretically an infinite number of terrain combinations over which a caterpillar or so-inspired robot could travel. Of course, simulating travel in every conceivable environment (with widely varying geometries) is impractical. Instead, this thesis proposes nonplanar environments can be well modelled by examining how effectively the caterpillar can transition between two planar surfaces, similar to the behavior shown in Figure 2. It is

hypothesized that the transition zone between the two planes can be modelled as geometrically similar to a circle.

As will be discussed in chapter 2a, Schuldt models caterpillar gait one-dimensionally, with compression taking the place of the vertical displacement typically seen in real-life caterpillars (this adaptation will be discussed in greater detail in Chapter 2A). This makes its adaptation to curved terrain non-intuitive. This thesis proposes that the terrain can be "flattened" by applying the curved terrain's biggest effects (gravity and curl of the caterpillar's body) to the same model Schuldt uses. Like Schuldt's model, travel will be expressed in one-dimension displacement and velocity. Unlike his, however, linear displacement will represent circumferential travel around a curved course. If a steady gait is observed (albeit with some more irregularities due to the curved terrain), that gait will be deemed successful. If successful gait is observed over a wide range of system design parameters, then the controller can be described as *robust*.

The focus of this work is to adapt Schuldt's model and assess the robustness of reflex-based gait in curved terrain. Specifically, this dissertation presents two contributions:

1. Proposed that crawling on non-planar terrain can be modelled one-dimensionally by accounting for changing gravity and body distortion from curling.
2. Demonstrated, utilizing this non-planar model, that reflex-based crawling can be robust on a wide array of non-planar terrain.

E. Guide

The end-goal of this thesis is to demonstrate that Schuldt's model can provide for robust locomotion in varied terrain. To this end, a computational code was written in Matlab to

simulate the crawl of a similarly-modeled robot. The remainder of the thesis details modeling and simulation tools, as well as their application to investigate robustness to different design and environmental parameters.

- Chapter 2 describes the development of the models and code utilized to movement on planar terrain. The algorithm is validated by comparison to Schuldt's prior results.
- Chapter 3 discusses the novel contributions of this thesis. It discusses the proposals outlined in the contribution 1 and discusses the steps necessary towards adapting the model to crawl over curved terrain. It is broken up into two subsections: "gravity" and "geometry." The gravity subsection looks at the implications of modifying the value of nondimensional gravity term in the governing equations. The geometry subsection examines the limitations of robot geometry on its ability to transition quickly between two planar environments (i.e. travel through a tight corner). Key to this analysis is the robot's ability to continue travel without all crochets able to attach. Both subsections apply simulations to determine robustness.

The thesis ends with a concluding chapter summarizing its results and contributions. An appendix highlighting the code utilized follows.

2. Methods

To understand Schuldt's methods fully and to expand on them, a new simulation code was written. This section describes Schuldt's original model in detail and then outlines the methods used for simulation. Code validation is performed by comparing results of the new simulation code to the outputs from Schuldt's original code for crawling on flat or inclined terrain.

A. Schuldt's Model

Schuldt bases his model[13] on caterpillar anatomy by abstracting it into six body segments shown in figure 5. At the front or anterior end of a caterpillar is a series of segments known as the thorax. The model abstracts the thorax into a single lumped mass. Immediately to the rear of the thorax are four identical abdominal segments known by biologists as A_3, A_4, A_5, and A_6. At the rear or posterior is an additional segment known as the terminal proleg (TP). Together the lumped thorax, four abdominal segments and the terminal proleg are the six segments considered in Schuldt's model.

For the purposes of the describing each segment's displacement, the model defines a point on each segment. The points are labeled P_0 (for the thorax) through P_5 (for the terminal proleg). Note that the numbering scheme used for dynamic modeling (segments indexed 0 through 5) is different from the numbering scheme used by biologists (e.g., abdominal segments A_3 through A_6). In the model, segments are linked by a series of springs, dampers, and muscles (Figure 6). Among the six segments present in the model, the thorax is unique in that it lacks a crochet, the gripper that allows the caterpillar to crawl. The practical implication of this is that the thorax can't anchor itself, and is assumed to be free to move back and forth

during simulated motion. Further, while there is a spring and a damper between the thorax and abdomen, no muscle is modeled at this connection.[i] Each segment is assigned an equal mass *m* and rest length $\bar{l}$ (in this model, the segments are represented as point masses collocated with its crochet; the rest length represents the distance between two crochets). While the thorax is significantly larger than the other segments in actuality, it is assigned these same characteristics for simplicity.

Figure 5 Anatomical diagram of the caterpillar with segment labels and incline label (modified public domain image from commons.wikipedia.org) [27]

[i] Despite this, Schuldt does, in fact, plot muscle 1, although he assumes it to play no role. No such muscle will be plotted in this thesis.

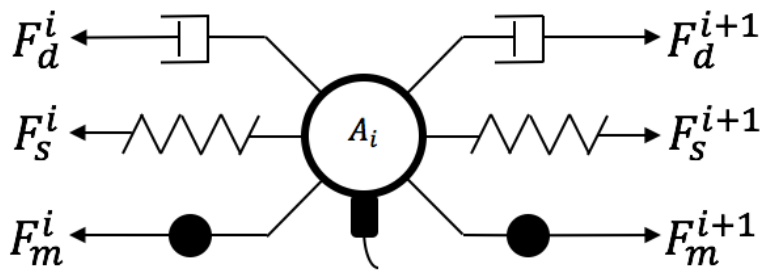

Figure 6 Free-body diagram showing forces acting on each abdominal segment. The lower two arrows with the dots represent the muscles, with the spring and dampers shown on the middle nad top arrows, respectviely. When the crochet is engaged, it exerts a force sufficient to restrict segment acceleration to 0[1]

For the non-boundary segments, dynamics are dictated by a force balance between the springs, dampers, and muscles fore and aft of a given segment. The spring force for a given segment *i* is defined by:

$$F_s^i = -k_i\left(l_i - \bar{l}\right) = -k_i\left(p_i - p_{i-1} - \bar{l}\right) \tag{1}$$

where k_i is the spring rate, modelling the elasticity of each body segment. The damper force is similarly defined by:

$$F_d^i = -c_i \frac{dl_i}{dt} = -c_i(v_i - v_{i-1}), \tag{2}$$

where c_i is the damping coefficient. Finally, the muscle force is defined by a step input:

$$F_m^i = \begin{cases} 0 \ \phi_i = 0 \\ A_i \ \phi_i = 1 \end{cases} \tag{3}$$

where A_i is the magnitude of the muscle force and $\phi_i = 1$ indicates that the referenced segment's muscle is activated. Thus, the dynamic equation for a given body segment can be represented by:

$$m\ddot{p}_i = \left(F_s^i - F_s^{i+1}\right) + \left(F_d^i - F_d^{i+1}\right) + \left(F_m^i - F_m^{i+1}\right) + \kappa_i - mgsin(\theta). \tag{4}$$

where κ_i represents the force exerted by the crochet and θ represents the incline encountered by the caterpillar, as shown in Figure 5. The relationships between the fore/aft spring and damper forces can be simplified by using a discrete Laplacian operator (∇^2):

$$\nabla^2 p_i = -p_{i+1} + 2p_i - p_{i-1} \tag{5}$$

$$\nabla^2 \dot{p}_i = -\dot{p}_{i+1} + 2\dot{p}_i - \dot{p}_{i-1}. \tag{6}$$

Applying the Laplacian and assuming constant damping and spring coefficients as well as muscle force magnitudes between all segments (except at the junction between the abdomen and thorax) simplifies equation 4 to:

$$\ddot{p}_i = -\frac{c}{m}\nabla^2 \dot{p}_i - \frac{k}{m}\nabla^2 p_i + \frac{A}{m}(\phi_{i-1} - \phi_i) + \frac{\kappa_i}{m} - gsin(\theta). \tag{7}$$

In order to reduce the number of parameters considered in evaluating robustness, Schuldt introduced the following non-dimensional parameters:

$$\zeta = \frac{c}{2\sqrt{mk}} \tag{8}$$

$$g = \frac{mgsin(\theta)}{A} \tag{9}$$

$$K = \frac{\kappa}{A} \tag{10}$$

Utilizing these non-dimensional parameters, equation 7 becomes:

$$\ddot{x}_i = -2\zeta\nabla^2 \dot{x}_i - \nabla^2 x_i + (\phi_i + \phi_{i+1}) - g - K_i. \tag{11}$$

As described later, the gripper force acts as a constraint rather than a force when engaged. Conversely, it can be assumed to be zero if the gripper is free. Eliminating the gripper force K_i from equation 11, only two dimensionless parameters remain, the damping ratio ζ and the dimensionless gravity g. Thus, not including parameters used for control, only two parameters need to be varied to assess the robustness of the baseline crawling model.

It should be noted that the thoracic segment has a slightly different governing equation. Because the thoracic mass lacks a crochet and cannot anchor itself, and because there is no muscle force between it and A_3, the thoracic mass effectively exists as a push cart (as in it is "pushed" by the segment behind it and doesn't provide any motivating force to the segments behind it) on the front of the system. For this reason, the governing equation for A_0 is:

$$\ddot{x} = 2\zeta(\dot{x}_1 - \dot{x}_0) - \left(x_1 - x_0 - \bar{l}\right) - g \text{ (12)}^{\text{ii}}. \tag{12}$$

Gait is achieved by utilizing a hybrid control law to control the muscles and crochets.

The system's passive dynamics, described by equations 11 and 12, are actuated by three control inputs: the motion of the TP (which is modeled as a boundary condition), the action of the crochets, and the action of the muscles. The motion of the TP, described by position variable x_5, is simply prescribed as a step change that initiates gait.

$$x_5 = \begin{cases} 0 & t = 0 \\ x_{init} \cdot \bar{l} & t > 0 \end{cases} \tag{13}$$

Now consider the action of the crochets, which lock and unlock based on a series of thresholds, Λ_{pos}, Λ_{vel}, and Λ_{acc}. The "unlock" condition on the crochet is based on the static force balance, which can be expressed by a simplified version of equation 11:

$$K_i = -\nabla^2 x_6 + (\phi_5 + \phi_6) - g,^{\text{iii}} \tag{14}$$

In this equation, the $\nabla^2 \dot{x}_i$ term (seen in equation 11) drops to 0 since there is no velocity. If the force K_i computed from equation 13 becomes larger than a preset threshold Λ_{aac}, then the crochet switches from the "locked" to "unlocked" condition.

[ii] This equation differs from Schuldt's; his paper shows the equation with a negative sign in front of $2\zeta(\dot{x}_1 - \dot{x}_0)$.

[iii] This equation also differs, but because Schuldt lacks a negative sign on $-\nabla^2 x_i$. In both cases, experimentation produced much more reasonable results with the noted changes.

In order for a crochet to relock, three conditions must be met. The acceleration (as outline in equation 11) must fall below Λ_{acc}, so as to ensure re-latching doesn't cause damage to the crawler (as stopping a segment moving under high acceleration would require high internal reaction forces that could tear the crawler apart). The velocity must also fall below the Λ_{vel} threshold. Finally , the distance between the segments fore and aft of a given crochet must exceed a threshold known as Λ_{pos}, which is defined as a fraction of the segment's rest length.

In a physical system, the crochets would only be able to relock when they were within a certain distance of the substrate. Given that the model is one dimensional, and that distance from the substrate is not explicitly modeled, the position threshold described above serves as a proxy for how close the crochet is to the substrate. The theory behind this is that a caterpillar displaces its body segments upward when segments approach each other. If the segments were rigid, then the positions on the substrate would form the base of a triangle shown in figure 7 from which height can be inferred through trigonometry. Because the segments are soft, the proximity condition is considered to be satisfied when the distance between segments is longer than the threshold Λ_{pos} (which is assumed to be somewhat smaller than twice the rest length). The crochet control law is summarized in figure 8.

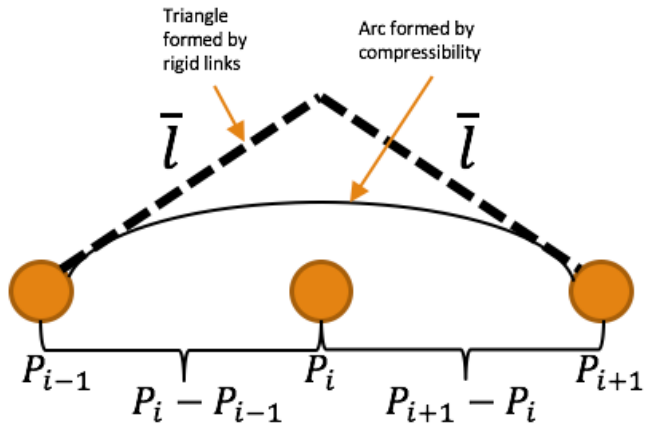

Figure 7 Detailed diagram of segments at rest (L) and approximation of vertically displaced body segments onto substrate (R) when in the free state.

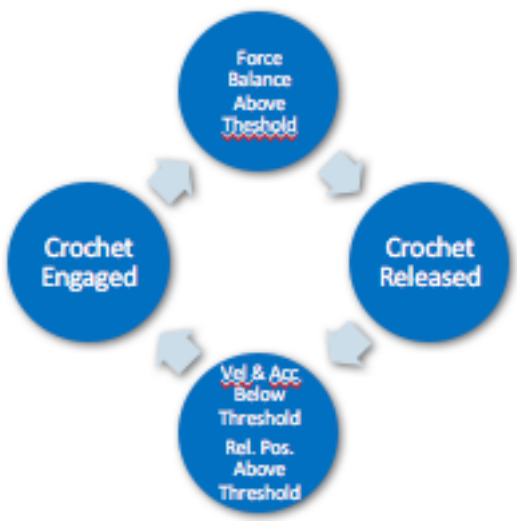

Figure 8 The crochet control law

The muscles are modeled as a *reflex-based* controller, meaning a controller that responds to local proprioceptive sensing (as opposed to control by a central pattern generator). The muscles activate based on the distance Laplacian (equation 5). The Laplacian operator acts as a simple model of local proprioception sensitive to differential strain. For example, if the distance between A_5 and A_6 is greater than that between A_6 and the terminal proleg, the muscle between A_5 and A_6 will fire, bringing A_6 forward (the muscle deactivates as soon as the

Laplacian flips from a negative to positive value). The control law for the muscles is shown in figure 9.

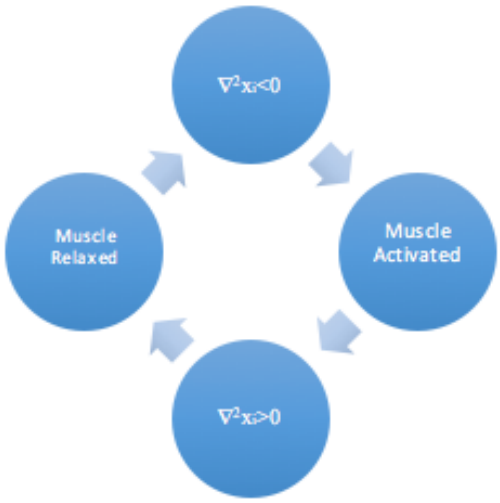

Figure 9 Muscle Control Law

B. Gait

This section qualitatively describes the crawling gait expected for the system model described above. This qualitative description bears a strong resemblance to the crawling kinematics of actual caterpillars, as observed by biologists in the lab.[xvi]

The gait cycle begins when the terminal proleg is moved forward. The forward displacement of the terminal proleg causes compression on the spring linking it to the neighboring abdominal segment (illustrated as A_6 in Figure 5) causing it to be subjected to an unbalanced force (if not for the crochet, which restricts its acceleration to 0). If expression 13 exceeds a predetermined threshold, Λ_{acc}, the crochet unlocks, allowing A_6 to travel forward. The forward motion is aided by the muscle between A_6 and A_5. This then creates an unbalanced force on A_5, which will cause its crochet to release, and the cycle repeats itself. The crochets

continue to unlock in an anterograde wave until A_3 releases, causing motion in the thoracic mass (whose motion is unchecked by a muscle or crochet) that closely follows that of A_3.

The terminal proleg serves as the anchor for the entire gait cycle. As the segments begin to reach a new positional equilibrium, their respective crochets relock, starting with A_6 and working forward. The sequence of reattaching begins prior to A_3 unlocking. Once all of the segments relock, the terminal proleg displaces forward again, and the cycle repeats.

C. Code Development

As discussed in chapter 2a, the dynamics of an abdominal segment are given by equation 11 (with the thoracic mass governed by equation 12). Because of the coupled forces between segments, expressed through the Laplacian operators in equations 5 & 6, a state-space representation becomes useful. Combining equations 11 and 12.

$$\begin{bmatrix} \dot{x}_0 \\ \ddot{x}_0 \\ \dot{x}_1 \\ \ddot{x}_1 \\ \dot{x}_2 \\ \ddot{x}_2 \\ \dot{x}_3 \\ \ddot{x}_3 \\ \dot{x}_4 \\ \ddot{x}_4 \end{bmatrix} = \begin{bmatrix} 0 & 1 & 0 & 0 & 0 & 0 & 0 & 0 & 0 & 0 \\ 1 & -2\zeta & -1 & 2\zeta & 0 & 0 & 0 & 0 & 0 & 0 \\ 0 & 0 & 0 & 1 & 0 & 0 & 0 & 0 & 0 & 0 \\ 1 & 2\zeta & -2 & -4\zeta & 1 & 2\zeta & 0 & 0 & 0 & 0 \\ 0 & 0 & 0 & 0 & 0 & 1 & 0 & 0 & 0 & 0 \\ 0 & 0 & 1 & 2\zeta & -2 & -4\zeta & 1 & 2\zeta & 0 & 0 \\ 0 & 0 & 0 & 0 & 0 & 0 & 0 & 1 & 0 & 0 \\ 0 & 0 & 0 & 0 & 1 & 2\zeta & -2 & -4\zeta & 1 & 2\zeta \\ 0 & 0 & 0 & 0 & 0 & 0 & 0 & 0 & 0 & 1 \\ 0 & 0 & 0 & 0 & 0 & 0 & 1 & 2\zeta & -2 & -4\zeta \end{bmatrix} * \begin{bmatrix} x_0 \\ \dot{x}_0 \\ x_1 \\ \dot{x}_1 \\ x_2 \\ \dot{x}_2 \\ x_3 \\ \dot{x}_3 \\ x_4 \\ \dot{x}_4 \\ \dot{x}_5 \end{bmatrix} + \begin{bmatrix} 0 \\ \bar{l} - g \\ 0 \\ (\phi_0 + \phi_1) - g \\ 0 \\ (\phi_1 + \phi_2) - g \\ 0 \\ (\phi_2 + \phi_3) - g \\ 0 \\ (\phi_3 + \phi_4) - g + x_5 \end{bmatrix} \quad (15)$$

where the index *i* corresponds to the segment indices 0 through 5 (as used to describe P_0 through P_5 in Figure 5). As discussed previously, the dynamic equations, and therefore the state-space representation, apply only when a given segment's crochet is unlocked. In other words, there are periods where $\ddot{x}_i = \dot{x}_i = 0$ for one or more (and possibly all) values of i.

Ignoring the muscles and the crochets, this system is relatively straightforward to simulate using one of the built-in ODE solvers in Matlab[28], such as ODE45, as all that remains are springs and dampers (which can be represented using a 1st order ODE).

The control law governing the muscle force, as outlined in chapter 2a, is dependent solely on whether the positional Laplacian, $\nabla^2 p_i$, is positive or negative (representing a lack of balance in relative position between a segment's neighbors fore and aft). This results in an instantaneous activation of the muscle. ODE45 is capable of handling this behavior, as the states referenced to control muscle activation are available within the function file. The muscles can be represented as a Boolean variable (where a "true" statement will output a 1), such as:

$$\phi_i = (\nabla^2 p_i > 0) \tag{16}$$

Unlike the muscles, which are modeled in equation 16, the crochets actually change the dynamics, such that the state updates for the velocity and position of a "locked" segment become zero. Dynamic systems in which the governing equations are themselves a function of time are called *hybrid systems*. The hybrid dynamics of this crawling model mean that simply calling a function file in the command line wouldn't be adequate. This is because the function file must be updated whenever the governing equations are changed. A simple numerical implementation might integrate the hybrid system by evaluating the correct dynamics at each time step using the first-order Forward Euler method. To obtain higher accuracy, an adaptive Runge-Kutta solver was used at each time step instead. Rather than code the Runge-Kutta solver by hand, ODE45 was used instead. This use of ODE45 at each simulation time-step is somewhat nonstandard, as typically (for non-hybrid systems) the ODE45 command is used to

integrate the system across many time steps at a time. The code implemented to advance through a series of time steps (using ODE45 to advance the simulation at each time step) will be referred to subsequently as the "loop solver" code. The time interval, equal to 0.005 in non-dimensional time units, was determined experimentally to optimize program run time while ensuring adequate resolution. Although here this method is utilized to "lock" and "unlock" the crochets (changing between a dynamic state and a static one), it could also be utilized to switch between a number of different dynamic equations or states. For example, to study a moving or non-rigid substrate, the "locked" condition could be replaced with the dynamics of the substrate (assuming they were known).

Each gait cycle is initiated by an advance of the terminal proleg. The terminal proleg is triggered to initiate based on two factors: the crochets having all successfully relocked and a certain amount of time passing since its last forward movement. Each crochet is assigned a dummy variable, set to zero initially. When the crotchet relocks after travelling forward, its dummy variable is set to one. Once all the dummy variables have been set to one, and a set time has passed (which prevents repetitive terminal proleg displacements in rapid succession), the terminal proleg displaces forward. The dummy variable serves as a proxy for ensuring the type 4 error (described later in section E) doesn't occur; if all the crochets fail to reengage, the dummy variable won't be changed, and the next gait cycle will never initiate.

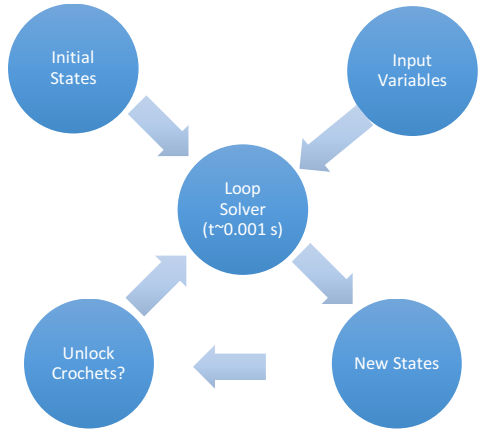

Figure 10 Flowchart outlining the loop solver code

D. Simulation of a Typical Gait Cycle

In order to run the simulation, specific values must be assigned to all parameters. The baseline parameter values used for simulations are reported in Table 1. The baseline parameters used here are identical to the baseline parameter set used by Schuldt[i]. By perturbing the baseline parameters over a wide range, it is possible to assess robustness (as will be described in Chapter 3).

Table 1 Nominal values for simulation, as specified by Schuldt.

Parameter	Nominal Value
ζ	1.5
g	0
x_{init}	0.4
$\bar{l}$	1
Λ_{acc}	0.2
Λ_{vel}	0.012
Λ_{pos}	1.4[iv]

[iv] Schuldt references this value as 0.7. However, the way the gating condition is written ($\Lambda_{pos} > x_{i+1} - x_{i-1}$), a value of 0.7 would correspond to the two segments being at 35% of their rest length, which is contrary to the logic of the controller. For this reason, 1.4 is used.

Simulating the caterpillar's motion utilizing the baseline values shows us what a "typical" gait might look like. The resulting states are shown in Figure 11, which shows six traces of segment position vs. time, in nondimensional units. The six traces are associated with segment 0 (the thorax) at the top and with subsequent segments shown in order moving downward to the bottom trace, describing segment 5 (the terminal proleg). For this demonstration, the simulation runs through eleven gait cycles. The bottom trace clearly shows that the terminal proleg is a simple boundary condition, implemented as a constant value with step changes corresponding to the initiation of each new gait cycle. The step change is smoothed out by the spring and dampers, so that the segments indexed 0 through 4 have smoother trajectories. The anterograde wave is clearly visible after the final step (on the right of Figure 11). In other words, the eleventh step is clearly visible at the bottom of the plot, where the terminal proleg trace makes its final jump before becoming flat. Each subsequent (moving aft to front) leg responds in sequence moving upward on the plot (toward the thorax on the crawler), with higher (more anterior) traces reaching equilibrium after lower traces.

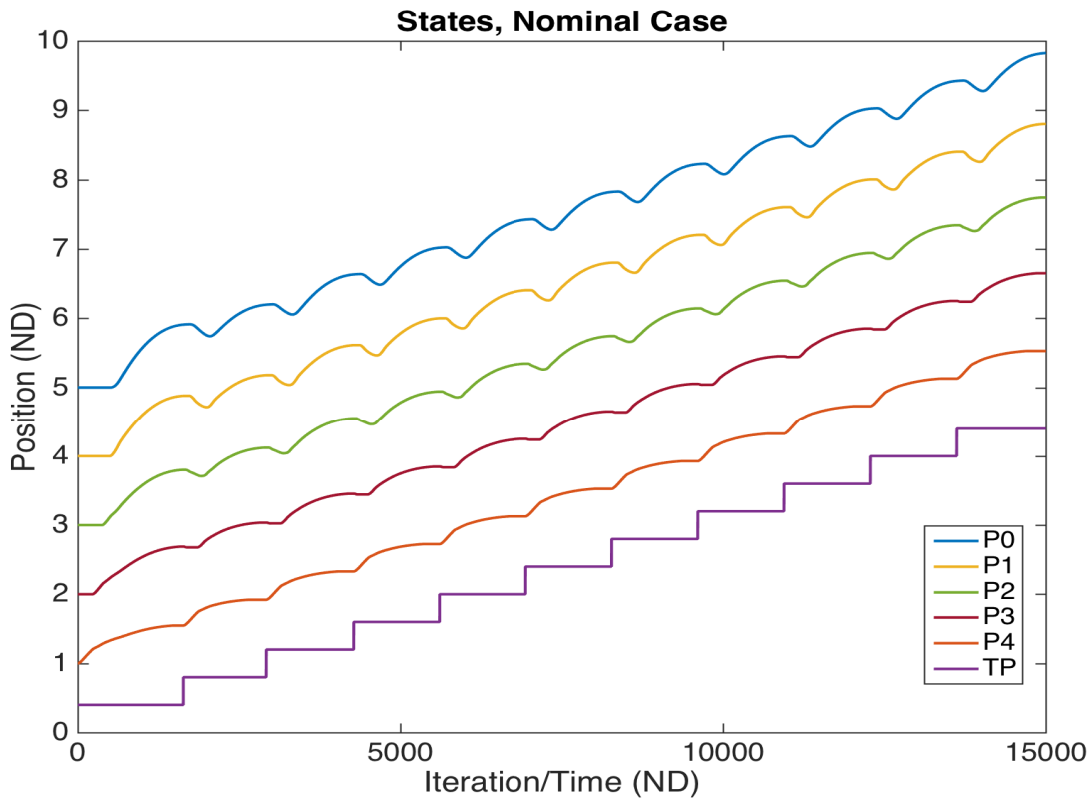

Figure 11 States, as solved for in the nominal case.

In order to understand nominal gait, it is also useful to examine characteristic crochet and muscle firing patterns. In figure 12, the typical engagement of the crochets through a simulation is plotted as a function of time. Each crochet's engagement is a binary value, where zero indicates unlocked and non-zero indicates locked. The non-zero (unlocked) values are set to different integers (1 through 4) corresponding to the segment index. These binary values are plotted against nondimensional time through 10 gait cycles. As seen in the position plot, the first gait cycle is longer than the others, as some earlier transient behavior has to die out before a regular gait can occur. This regular gait is seen in the subsequent gait cycles.

As the gait starts at the terminal proleg and proceeds forward, C_1 is the first to release. C_2, C_3, and C_4 then follow in order. Note that the numbering convention here (and for the

muscles and crochet plots throughout the thesis) goes from number 1 at the rear to 4 towards the front. As the gait cycle completes, the crochets then relock in order. The next gait cycle then begins, and the process repeats. The regularity of this plot helps confirm a successful gait.

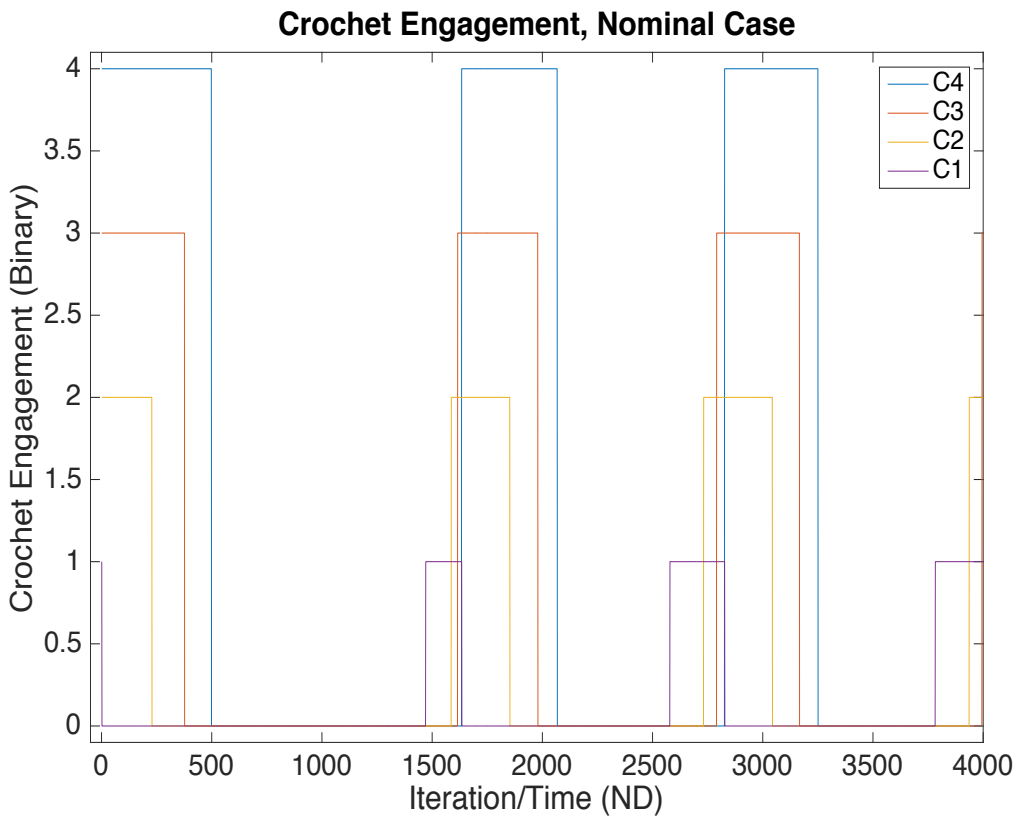

Figure 12 Crochet engagement over time in the nominal case (zoomed in to a smaller time interval for added detail. Binary values are multiplied by a different factor for visual clarity.

Figure 13 shows a similar plot for muscle activation. In much the same way, the plot shows four binary variables, where a nonzero value indicates muscle activation and a zero value indicates no activity. (For visibility, muscle activation values are again set equal to the index of the corresponding segment, 0 through 4). The simulation beings with all four muscles inactive. M_4, between the last two abdominal segments, activates first, and the sequence continues down the body. Once again, the regularity contributes to demonstrating a successful gait.

What can be seen modelled in figures 12-14 is an example gait consistent with what Schuldt describes.[2]

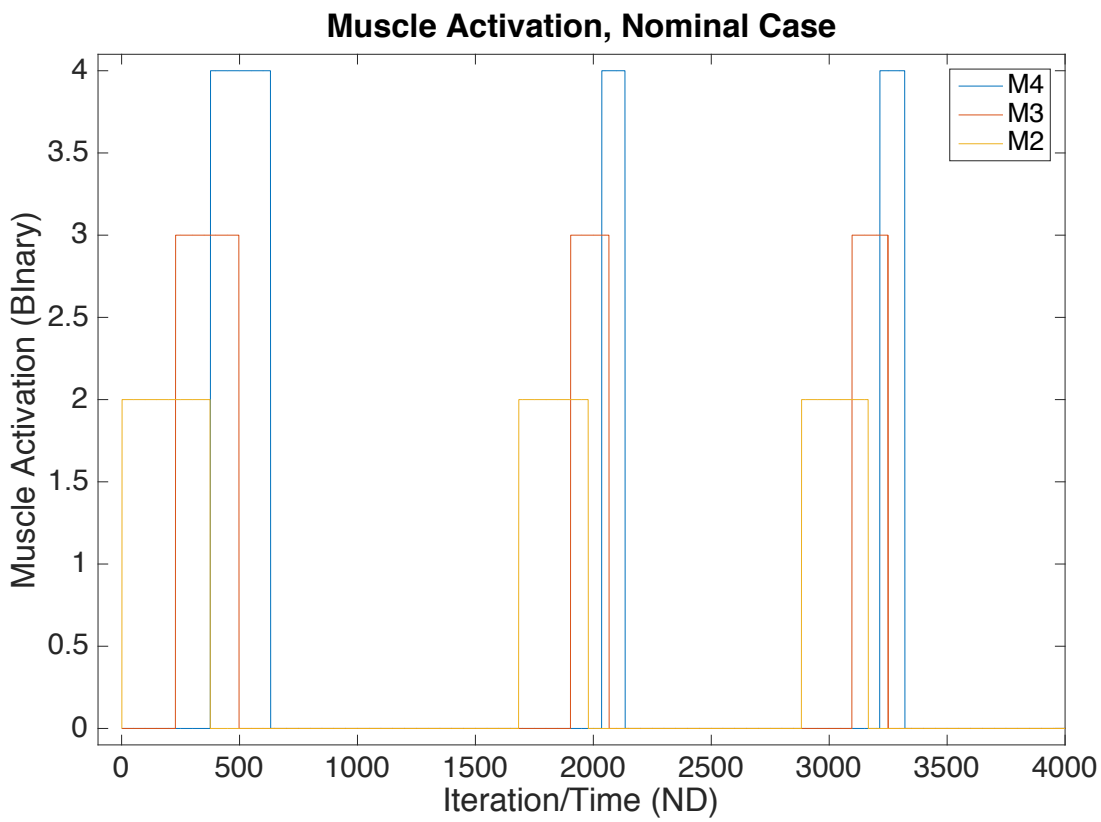

Figure 13 Muscle activation for the nominal case. Binary values are multiplied by a different factor for visual clarity

E. Identifying Successful Gait

For the proposed reflex-based controller to be useful, it should perform well not only in the baseline case, but also over a wide range of other scenarios, with different physical or environmental conditions. For each scenario, a formal definition is needed to describe whether or not the simulated gait is a "success" or a "failure." In his work, Schuldt defined gait failure as one or more of the following four events occurring.

Type 1: Anterograde wave not observed: failure of the muscles to fire in an aft-to-fore sequence.

Type 2: Segment order not preserved: segments cannot cross.

Type 3: Failure to converge to a steady crawl: gait cycles are supposed to be repeatable and consistent; segment lengths should converge to within 10% of their rest length after each crawl.

Type 4: Failure of crochets to reengage: the body segments are supposed to, at a certain point, concurrently all be in a state where their crochets are able to relock.

In this thesis, Schuldt's definitions are used to define "failure." Any event which is not a "failure" is considered a "success." It is worth noting that Schuldt's work relied on automated code to check for failure. A large number of simulations were run sequentially and plots of different variables were produced indicating which ones were successes and which were failures. For this thesis, each case was checked manually.

F. Code Validation

Because new code was developed to conduct the work described in this thesis, it makes sense to validate the new code by comparing its results to those of the original code used by Schuldt. Schuldt's original results identified whether or not simulated gaits were successful as simulation parameters were perturbed away from the nominal values given in Table 1. This resulted in what he referred to as "single parameter sensitivity."

Schuldt's procedure was to increment a parameter upward from its nominal value until either a gait failure was observed or a limiting value of the parameter was reached. Once failure was observed (and the upper bound of success for that variable found), the same procedure was then repeated while decreasing from the nominal value. The next variable was then tested (with the first returned to its nominal value). A comparison to Schuldt's results is shown in Table 2. For both sets of results, the acceptable variables are expressed as a range within which the model achieves successful gait.

Table 2 Results of the single parameter sensitivity study.

Parameter	Min (S)	Max (S)	Min (K)	Max (K)
$\boldsymbol{\zeta}$	+	+	0.2	+
$\boldsymbol{g}$	-0.26	0.15	-0.21	0.19
$\boldsymbol{x_{init}}$	0 (no crawl	1 ($\bar{l}$)	0 (no crawl)	0.99
$\boldsymbol{\bar{l}}$	0.1	+	+	+
$\boldsymbol{\Lambda_{acc}}$	-0.015	0.72	0.05	1.25
$\boldsymbol{\Lambda_{vel}}$	0.005	+	0.001	+
$\boldsymbol{\Lambda_{pos}}$	0	0.95	0	2

The results of the single parameter sensitivity study (with Schuldt's denoted by an S and this thesis' by a K) demonstrate that the simulations are similar, although not exactly the same due to differences in coding and numerical methods. Going line by line, the damping coefficient has the same upper bound (+, denoting no maximum limit), although there is a minimum bound for this paper's results where Schuldt's allow for any value greater than zero. g has almost identical ranges (0.41 vs. 0.4), and boundary values within 25% of each other. x_{init} is effectively equivalent, as a value of 1 in this model would result in two segments occupying the same point at the same time. $\bar{l}$ features a similar comparison as ζ, with the exception being increased robustness for this thesis over Schuldt's (between 0 and 0.1). Further, Schuldt enables $\boldsymbol{\Lambda_{acc}}$ to have a negative value, but the code developed for this thesis sets up that comparison using absolute values, making negative values impossible. Λ_{vel} has the same upper bound (there isn't one), and the lower bounds are at the same order of magnitude. The different interpretation in Λ_{pos} is explained in footnote 3 above. Taking that into account, the upper bounds are within 5% of each other.

Not all gait failures will occur by only varying one parameter. For this reason, Schuldt also examined the sensitivity of four parameters (ζ , Λ_{acc}, $\Lambda_{vel}, and\ \Lambda_{pos}$) at varying values of g. He utilized the automated validation code described previously to produce a series of plots describing his result exploring these four spaces. To further prove validity against Schuldt's results, a similar set of experiments were run with the loop solver. For each of the four spaces (the aforementioned four parameters vs. g), the simulation was run with one of the two variables set at its max value as found in the single parameter sensitivity study. Then, the boundary range of successful gait was found by incrementing one variable or both by 0.01. Earlier experimentation revealed that gait in the intermediate areas was "smooth", with consistently success. In other words, when any of the parameters were within the boundaries found here, there was only successful gait. For this reason, only the boundary plots are presented in this thesis.

The results showed that the loop solver could simulate robust gait over a wide range of parameters. Two of the four parameters, $\Lambda_{vel}\ and\ \Lambda_{pos}$, demonstrated no sensitivity to g; their minimum and maximum values were the same regardless of non-dimensional gravity. The damping ratio produced similar, albeit not exactly the same result. At high values of ζ, slightly lower (0.01 less) values of g is tolerated on the positive extreme. On the extreme of $-g$, there is no variation; the same value is tolerated across all values of ζ. The Λ_{acc} results were unique, in that, at low values, there is a very small range for g. As Λ_{acc} increases, the range increases linearly. Considering equation 11, this result is not surprising. Gait can only be successful when all of the crochets reach a point in the cycle where $\ddot{x} < \Lambda_{acc}$. If $g > \Lambda_{acc}$, the crochets can never relock, since $\ddot{x}$ is always greater than Λ_{acc}.

This process resulted in a series of plots that could be compared against Schuldt's results. In figures 15-18, the boundaries of the experiments performed for this thesis are overlaid over Schuldt's results (where success is shown in black).

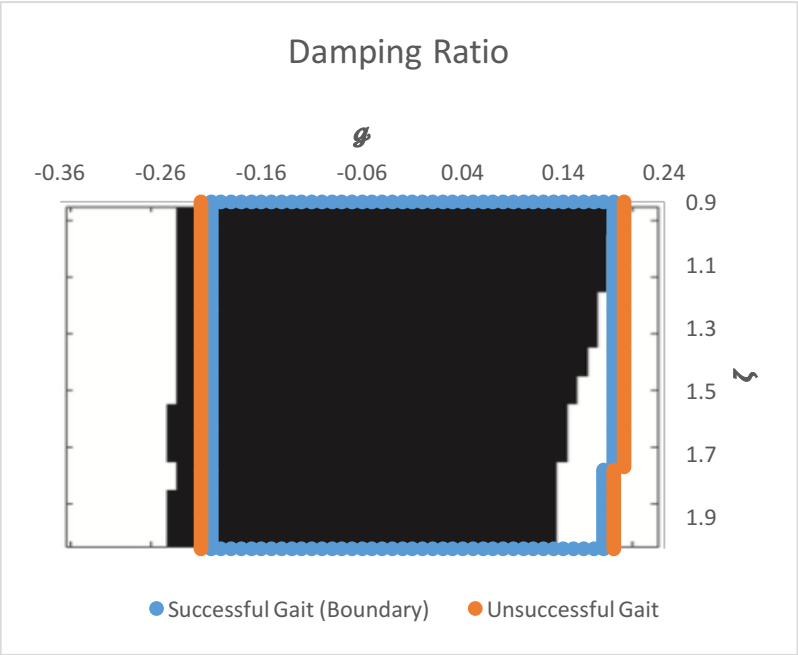

Figure 14 Boundary plot of damping ratio vs. non-dimensional gravity of successful gait superimposed over Schuldt's results.

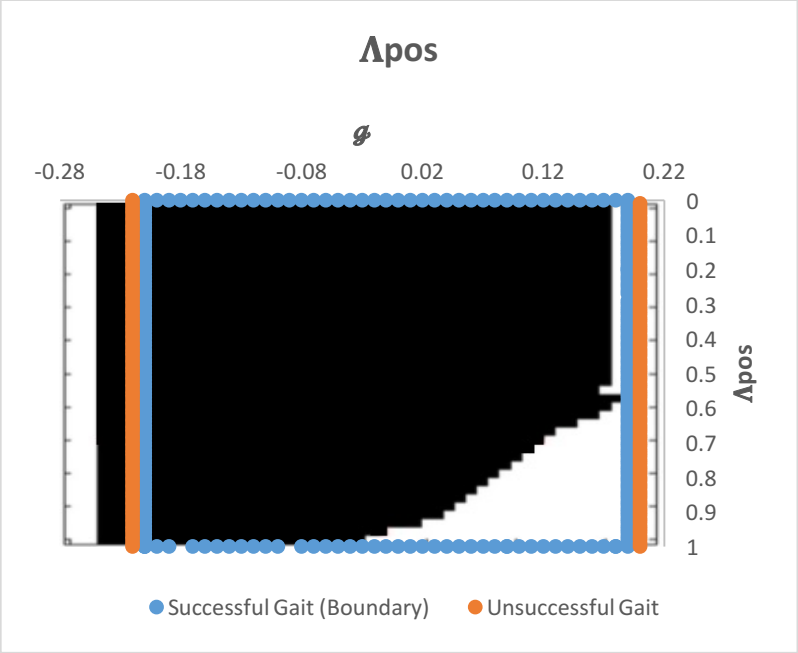

Figure 15 Boundary plot of Λ_{pos} vs. non-dimensional gravity of successful gait superimposed over Schuldt's results.

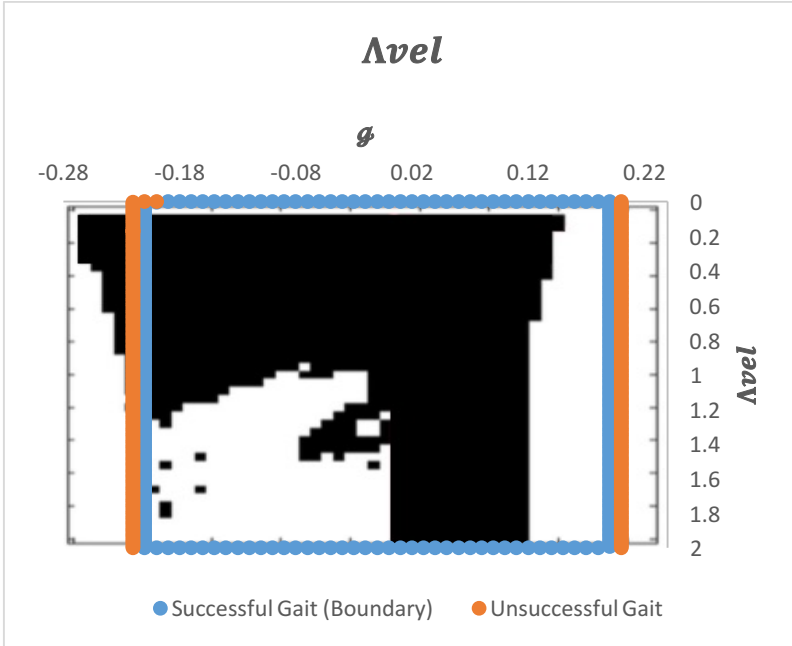

Figure 16 Boundary plot of Λ_{vel} vs. non-dimensional gravity of successful gait superimposed over Schuldt's results.

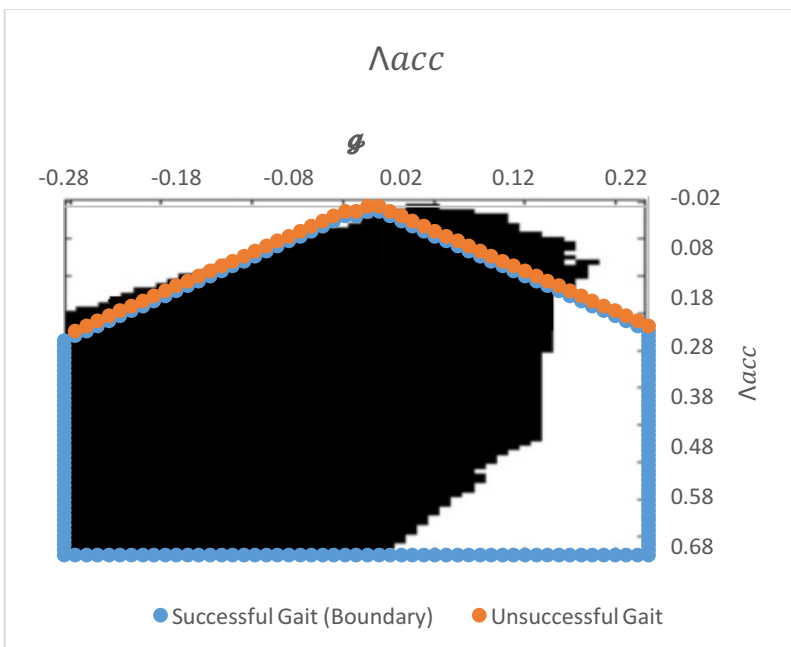

Figure 17 Boundary plot of Λ_{acc} vs. non-dimensional gravity of successful gait superimposed over Schuldt's results.

The totality of this validation work demonstrated that, while the model presented here didn't present the exact same results as Schuldt, there was a pattern of relative consistency in order of magnitude and numerical values that made the models comparable. The comparative

scale of the parameters between Schuldt's and this thesis have already been discussed in the single parameter sensitivity study. This gave confidence that the new model was in the same scale as Schuldt's. Looking at the comparison plots, damping ratio shows a similar shape to Schuldt's, while Λ_{vel} and Λ_{pos}show robustness in a new region (white space) in each that Schuldt's didn't. Perhaps most interestingly, the Λ_{acc} plot shows a similar "v" shape around the minimum value for both studies. However, the loop solver produces a "v" centered around $\boldsymbol{g}$ =0, while Schuldt's shows a bias in the positive $\boldsymbol{g}$ direction. This may be explained by the difference in interpretation of the Λ_{acc} parameter. In the loop solver, Λ_{acc} is checked against the absolute value of the acceleration, while Schuldt allows for negative values of Λ_{acc}. This difference likely allowed for the symmetry about zero in the new boundary plot. Like the other threshold parameters, the new boundary for Λ_{acc} has introduced a new region of robustness. The end result of this study is that the models are qualitatively, if not exactly quantitatively similar. The implication is that the models are similar, if not directly comparable. The goal of this thesis, however, is to expand upon Schuldt's work, and not to merely imitate it. The novel work presented in chapter 3 will make the issue of a direct numerical comparison a moot point, as the non-planar travel simulated there is fundamentally different than the results previously presented, making their exact comparison impossible.

3. Travel in Non-Planar Environments

This chapter will detail the novel work that leads to the thesis' main contributions. The chapter is broken into two sections, gravity and body distortion, to discuss the two main challenges of non-planar travel. Each of these sections is then broken into two subsections: one to discuss the model, and the other to discuss the results of implementing that model.

A. Gravity Implications

i. Modelling Gravity Variations

As mentioned previously, the addition of curved terrain into Schuldt's model has two major implications, with the first being the effect of changing gravity. Recalling equation 11, the obvious mathematical impact of varying gravity will be on the non-dimensional gravity term, g. g will now vary as θ changes. Consider the following path of travel:

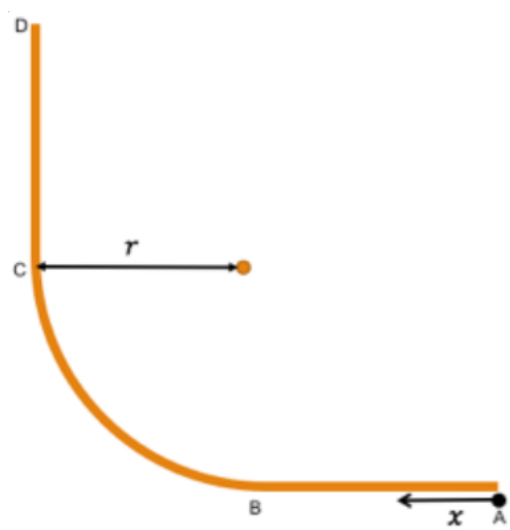

Figure 18 Example course of travel. In this scenario, the caterpillar starts at point A and travels towards point B, after which it climbs up the curved portion (fillet) and onto the vertical surface.

where the caterpillar walks from A towards D, there are effectively three different applications of equation 11 needed. From point A to point B, the equation applies with $\theta = 0$, and, thus, $g = 0$. From point C to point D, the same applies but now with $\theta = 90°$ and $g \neq 0$. From

point B, to point C, however, θ (and g) vary as the caterpillar travels forward. Further, θ varies between body segments while on the curve, which is not seen in Schuldt's work and necessitates the use a segment-specific inclination angle θ_i, where i=0, 1,...5 corresponding to the positional references P_0 through P_5.

Because gravity is segment specific, a new variable g_{max} was introduced to describe the environmental condition (e.g. the nondimensional gravity for motion on the vertical slope). A segment-specific nondimensional gravity can be computed from g_{max} as follows:

$$g_i = \begin{cases} 0 & x_i < L \\ g_{max} \sin \frac{x_i - L}{r} & L \leq x_i < L + \frac{\pi r}{2} \\ g_{max} & L + \frac{\pi r}{2} \leq x_i \end{cases} \tag{17}$$

where *x* represents the distance travelled along segment AB, *L* is the distance along the segment AB where the curve begins, and *r* is the nondimensional radius of curvature of the substrate in segment BC. Thus, equation 11 becomes:

$$\ddot{x} = -2\zeta \nabla^2 \dot{x}_i - \nabla^2 x_i + (\phi_i + \phi_{i+1}) - g_i - K_i. \tag{18}$$

It is important to note that the model given by equation 18 assumes that the crawler perfectly follows the substrate. This assumption breaks down if the radius of curvature is to small (e.g. if the curve becomes too sharp an angle), as will be discussed in Section B of this chapter.

In simulating crawling with segment-specific gravity, the baseline parameters were identical to those shown in Table 1, with two modifications. First, the radius of curvature parameter *r* is a new parameter, absent in the original table. The parameter *r* was assigned a baseline value of 1. This puts the radius of curvature equal to the length of one of the crawler's body segments, putting the sharpness of the corner somewhere in the middle of the extremes. At one extreme, where the terrain is completely flat, *r* approaches infinity; at the other

extreme, in a corner case, *r* approaches zero. Second, the environmental parameter g_{max} was specified at 0.1 (as the baseline gravity in Table 1 was $g = 0$, indicating a flat plane).

It is instructive to visualize the gait in the baseline case. Plots of state, crochet engagement, and muscle activation for the baseline parameter set were generated by implementing segment-specific gravity in the simulation tools described in Chapter 2. The results are shown in figures 19-21.

Gait appears to be affected little as the crawler progresses over the curve between the flat plane and the vertical plane. This regularity is evidenced by the position against time traces for each body segment, shown in Figure 20. For each trace, twenty-one steps are shown. This is more cycles than were shown in chapter 2. This allowed the crawler to reach a steady crawl on flat surface (so as to allow any transients to die out), traverse the fillet, and then travel on vertical terrain. This number of steps was chosen to allow the crawler to completely transition between the flat and vertical surfaces. As seen previously, the initial cycle is longer than the others, but this is a transient effect that is eliminated quickly. The primary difference caused by segment-specific gravity is seen in the length of each step. This effect is most prominent in the top trace (thorax) around τ=12000, as the caterpillar enters the curved section. Most noticeably, the distance covered by the thorax in each step gets slightly shorter in the fillet section before lengthening again during planar vertical climbing. This change in step length also occurs in other segments, though the effect is less prominent moving posterior toward the TP. The net result of the shortened steps is that the crawling model gets slightly shorter during the transition from horizontal to vertical crawling (with the total length between P_0 and P_5 decreasing from 5.5 when the thorax enters the corner to 4.7 when the TP leaves the corner).

Pointers show the position of the extremes of the caterpillar's body at three points: prior to the fillet, while the middle segments are on the fillet, and on the vertical surface. The beginning and end of the fillet are shown with black lines.

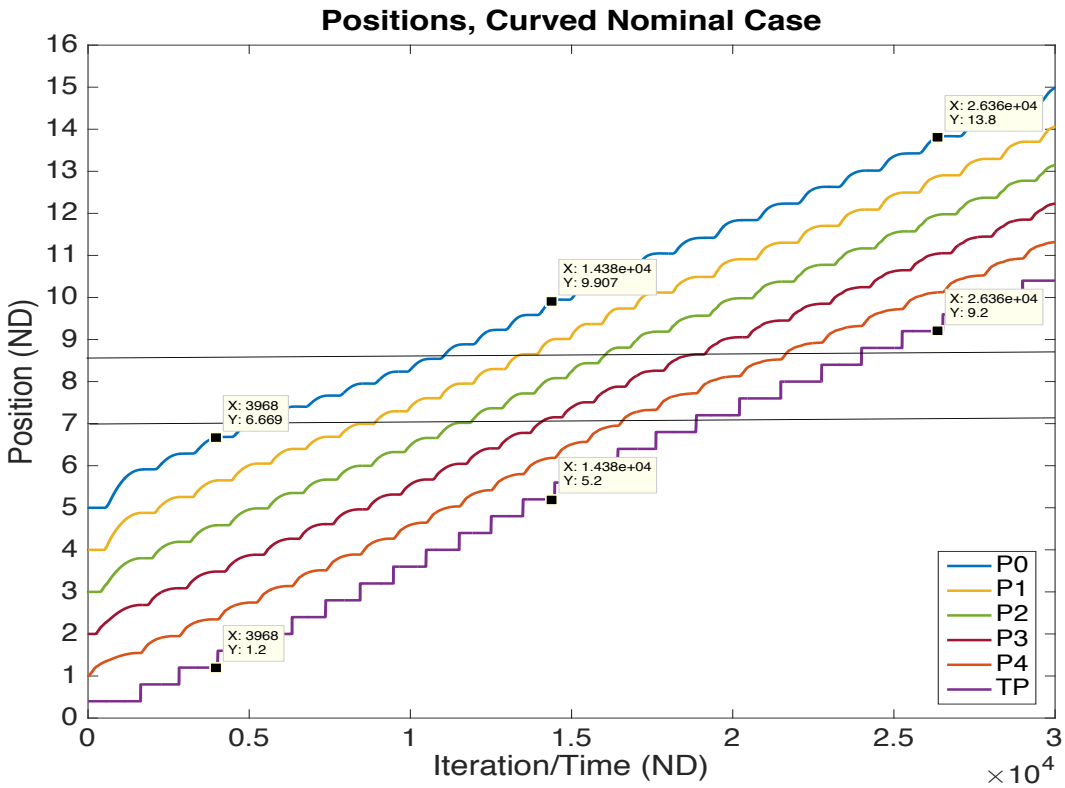

Figure 19 States vs. iteration as the caterpillar traverses the course.

Figure 20 shows the crochet engagement from τ=10000 to τ=15000, during which the caterpillar enters the curved surface. As in the flat case, we start with a regular pattern (gait cycle) of crochets 1, 2, 3, and 4 unlocking (where zero signifies unlocked) in order, where the high value indicates the crochet is locked. When the caterpillar hits the curve, however, some chatter is seen in crochet 1. This does work itself off, and the chatter is no longer seen by the final gait cycle in the plot. There is some slight chatter in crochet 2, which is also transient.

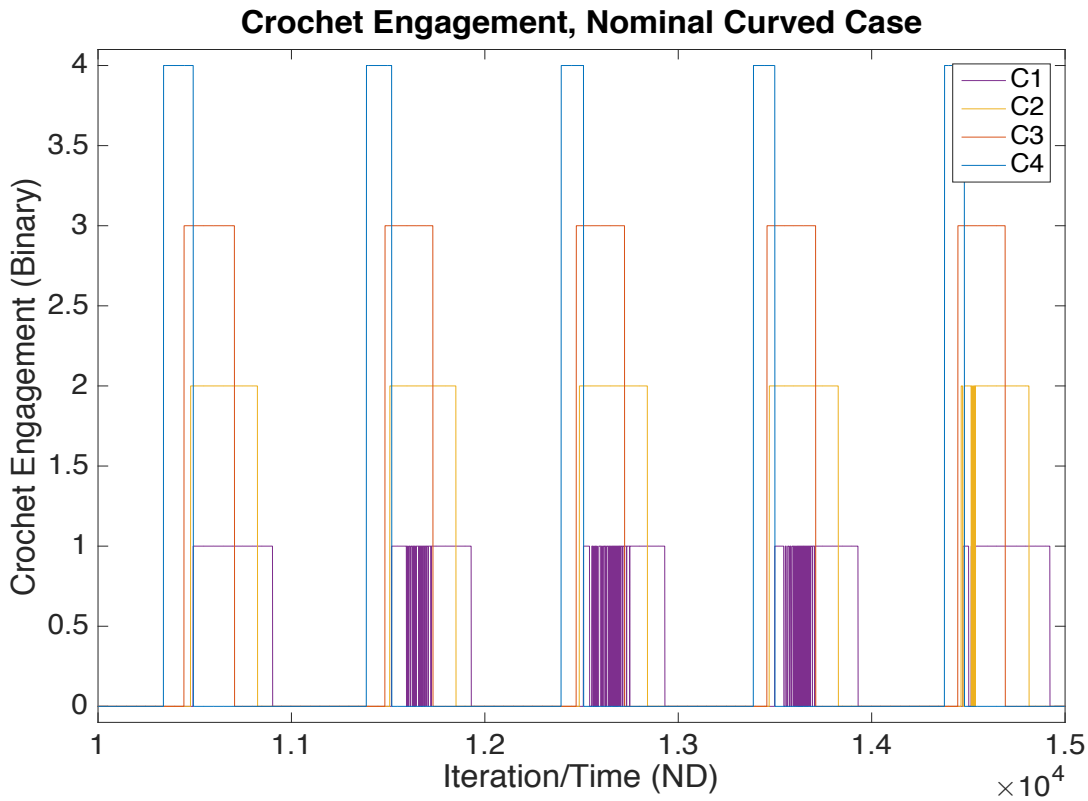

Figure 20 Crochet engagement through the nominal curved simulation. As in prior plots, the binary variable is multiplied by a constant for visual clarity.

Figure 21 shows the muscle activation plot over a similar interval (where high equals muscle activated and zero equals relaxed). Like the crochet plot, the same pattern of regularity starting at the back (muscle 2), and working its way forward, is seen. Again, there is some chattering as body segment A_4 (indexed as 2 in the model) reaches the curved surface. There is no muscle 1 shown, as there is no muscle between A_1 and the thorax.

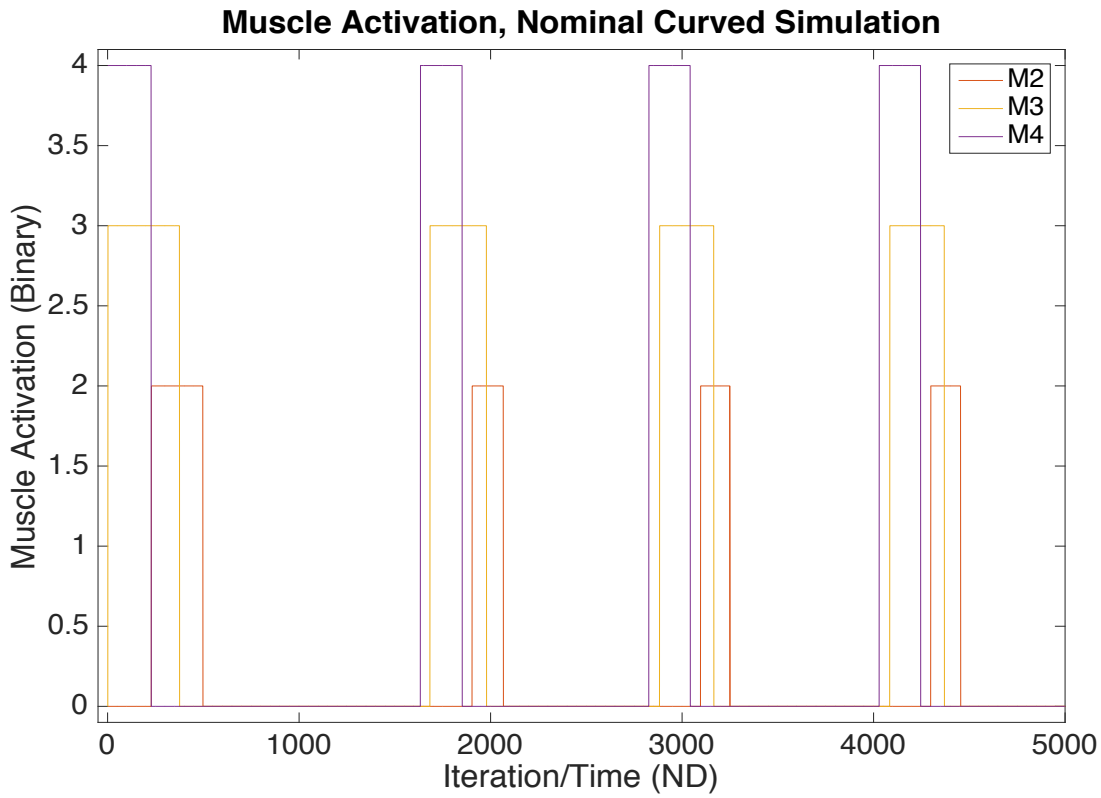

Figure 21 Muscle activation through the curved simulation. As in prior plots, the binary variable is multiplied by a constant for visual clarity.

Additionally, the segment-specific nondimensional gravity g_i was plotted over time, as shown in figure 22. The plot shows each segment faces increased gravitation along the axis of motion with each gait cycle taken on the corner section. As segments transition across the corner region, segment-specific gravity increases from 0 to g_{max} (0.1 in the baseline case). At any time in this nominal simulation, there were never more than two body segments in the corner region (as evidenced by the fact that there are never more than two traces with segment-specific gravity above zero and below g_{max} at the same time). This result is expected for a scenario with radius of curvature *r* = 1, which corresponds to the filleted section having an arc length of 1.57 (about one and a half times as long as a single body segment).

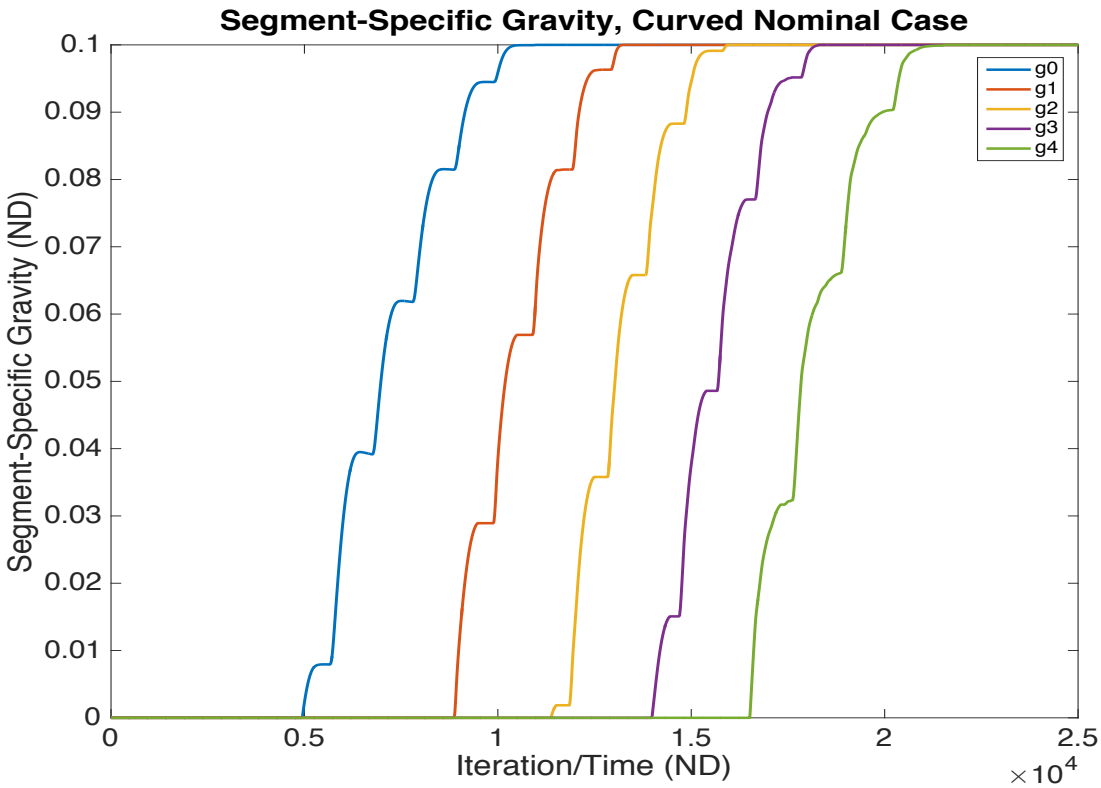

Figure 22 Segment-specific gravity (g_i) throughout the curved simulation.

The inspection of the four preceding plots, showing steady positive displacement, anterograde muscle and crochet firing, and steady increase in gravitational resistance, indicate a successful and robust gait, where success was defined by the criteria introduced in Section 2.E

ii. Robustness for Segment-Specific Gravity

In order to assess the impact of segment-specific gravity on the robustness of the crawling gait, success was evaluated for the non-planar substrate model over a range of curvatures and values of g_{max}. Other parameters were held to their nominal values as listed in Table 1. Results were compared to the planar model from Chapter 2.

A plot showing the boundary of successful gait in the space of g_{max} vs. radius of curvature (where radius=0 is the corner case) space is shown in figure 23. Three colors are present on the graph. The blue line corresponds to the boundary of gait success. Similar to the

boundary plots presented in chapter 2, gait was found to be consistently successful within the intermediate region. The orange line corresponds to the inner boundary of the region of gait failure. The grey region corresponds to successful gait in the planar case (where only g can vary). The negative values of g_{max} represent a course where the caterpillar starts horizontally, but goes down a curve onto the vertical segment, as opposed to up in Figure 18.

Gait was found to be successful at all radii of curvature for the same values of g found in the single parameter sensitivity study. In simulation, it was observed that robust gait can only occur when g_{max} can't exceed the values of g found in the single-parameter sensitivity study summarized in table 2. This is fairly intuitive, as travel along segment CD is the same as a straight-line course with $g = g_{max}$. The bottom-line for the robustness analysis is that gait success does not depend on radius of curvature when the rounded corner is modeled with only segment-specific gravity. Robustness for this model depends only on g_{max}, with dependence of gait success on gravity essentially identical to the planar analysis from Chapter 2. These results show that, with regards to the effect of changing gravity, the model is in the non-planar scenario across a wide range of curvatures.

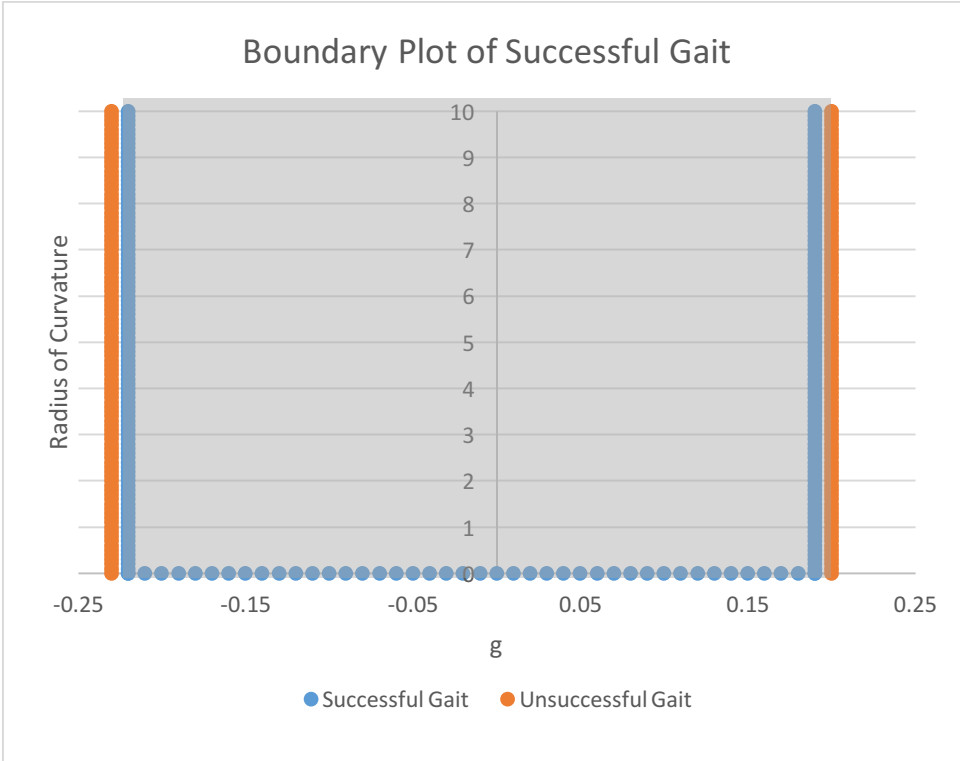

Figure 23 Boundary of successful gait within the a space of g_{max} vs. radius of curvature parameters. The grey region corresponds to successful gait in the planar simuation.

B. Geometry Implications

The experiment discussed in chapter 3a was successful with g_{max} set at both limits of g (-0.22, 0.19) as well as all values in between. There are, however, additional factors to consider. Up until this point, all experiments have been based on the assumption that the crawler will perfectly follow the substrate. This assumption is reasonable for many curved surfaces, but, at the extreme case, a sharp 90° corner, the crawler's body structure would prevent it from following the substrate perfectly. The 1-D crawler model proposed by Schuldt and expanded upon here doesn't account for body thickness or how much the body can "curl" about the z-axis (if we assume that the z-axis comes out of the page in the course diagrams presented in this thesis). In a 3-D model, these limitations would need to be addressed (prior

work has already demonstrated that having joints about which a robot can curl are beneficial in transiting non-planar terrain[29,30]).

Chapter 3a discussed abstracting the transition region between two planes as a curve or fillet, defined by radius of curvature *r*. The curling behavior discussed in the last chapter would likely be dependent on three factors: segment rest length ($\bar{l}$), segment thickness (the size of the body dimension perpendicular to the substrate), and segment flexibility (how much the segments can bend relative to each other). In order to account for these limitations, a new parameter, r_{min} was needed. This specifies the maximum radius of curvature to which the crawler can curl without breaking.

When $r<r_{min}$, there will be two fundamental differences separating the simulation from prior ones shown in this thesis. First, as mentioned previously, the crawler won't follow the substrate. This means that the caterpillar will have to follow a different course (hereinafter referred to as the "alternative course"), where segment-specific gravity doesn't correspond to the substrate (referred to as "travelling on the alternative course"). Two different alternative courses, referred to as the "inside case" and the "outside case" (based on whether the crawler is transiting the inside of a corner or the outside, see Figure 24) will be discussed in detail in the coming sections. The second pertains to the grippers. When on an alternate course, certain grippers won't be able to engage. When this occurs, gait success will be dependent on the other grippers (which are still on the substrate).

For simulation, a baseline value of r_{min} needs to be established. In order for gait to continue when some of the segments are on the alternative course, the distance between the crawler's first and last gripper (on A_3 and the TP respectively) must be longer than the

alternative course itself. This ensures that there is always a gripper on the substrate. This length corresponds to $4\bar{l}$ (or, for a caterpillar of *n* segments, [n-2]* $\bar{l}$). The length for the inside alternative course is equal to $\frac{\pi r_{min}}{2}$, while the inside's is equal to $\frac{5\pi r_{min}}{2}$ (justification for these expressions will be presented in the coming sections). To keep the simulations consistent, a single baseline value of r_{min} will be utilized to explore both cases. For this reason, the relation $4\bar{l} > \frac{5\pi r_{min}}{2}$ is utilized to determine r_{min}. This expression simplifies to $\frac{8}{5\pi} > \frac{r_{min}}{\bar{l}}$. With $\bar{l}$=1, r_{min}<0.51. With this in mind, r_{min}=0.5 will be utilized as the nominal case. Beyond the simulations for this thesis, this is an important consideration for real-life implementation of the model.

Figure 24 Inside/convex case (left)) vs. outside/concave case (right).

i. The Inside Case-Model

For the inside case, I proposed a course similar to that proposed in chapter 3a, but with the crochets unable to grip while on the curved portion of the course (which has a larger radius of curvature than the physical substrate). Effectively, the caterpillar approaches the curve, senses $r<r_{min}$ (through a sensing suite whose specification goes beyond the scope of this thesis), and curls in the negative Z direction (with +Z out of the page). While a body segment is on the alternative course, its crochets can't grip, and gait is maintained through the activity of the rear

segments still on the ground (travelling from A to B). Eventually, the forward segment passes point C onto the vertical portion, and the forward crochets begin reengaging. These segments then assist the rear segments as they transition through the "crochet-less" part of the course, equivalent to the fillet in the gravity model. It is important to note that, while a right angle is shown here, this scenario is applicable to the whole range of $r<r_{min}$.

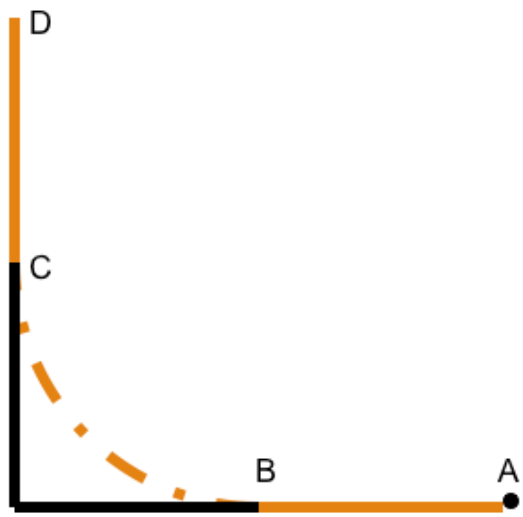

Figure 25 The inside alternative course. The robot travels normally from A to B and from C to D. Travel between B and C along the dashed line occurs without the crochets, which are unable to engage.

To simulate the inside course, a new parameter for r_{min} was entered into the loop solver. If $r<r_{min}$, then the course file was set up to return g_i consistent with a curved course with $r=r_{min}$. In other words, the crawler will approach the corner, sense a need to curl upward, curl to r_{min}, and proceed forward until A_3 reaches the vertical surface, allowing its crochet to engage, pulling the crawler upward. r_{min} must be set such that the path from B to C doesn't exceed $4\bar{l}$. If BC were to be longer than $4\bar{l}$, the crawler would have all its crochets off the surface, making travel impossible. As discussed previously, $\frac{\pi r}{2} < 4\bar{l}$.

ii. Inside Case-Validation

The inside case model was simulated utilizing the loop solver (with requisite modifications made to account for the differing segment-specific gravity and certain crochets being off the substrate). Resultant positional states from simulating the inside case are shown in figure 26. For comparison, a simulation was run with the fillet's radius of curvature set to r_{min}, with resultant states shown in figure 27. In this scenario, the crawler would be able to stay on the substrate throughout the entire simulation, but would have the same segment-specific gravity as the inside case with $r<r_{min}$. This allows for a more qualitative validation of the inside simulation results. More gait cycles are shown here than in previous plots to allow travel on the flat plane to eliminate startup transients, traverse the curve, and have sustained travel on the vertical surface.

Using the criteria discussed previously, both figures 26 and 27 show a robust gait. Further, the crawler progresses through the gait cycles similarly in both simulations. What this is shows is that the model can lose crochet engagement on one (or more) crochets and still maintain a robust gait. Further, this gait is effectively the same as when the crochets can continually engage. This shows that the model is robust against temporary loss of gripping ability.

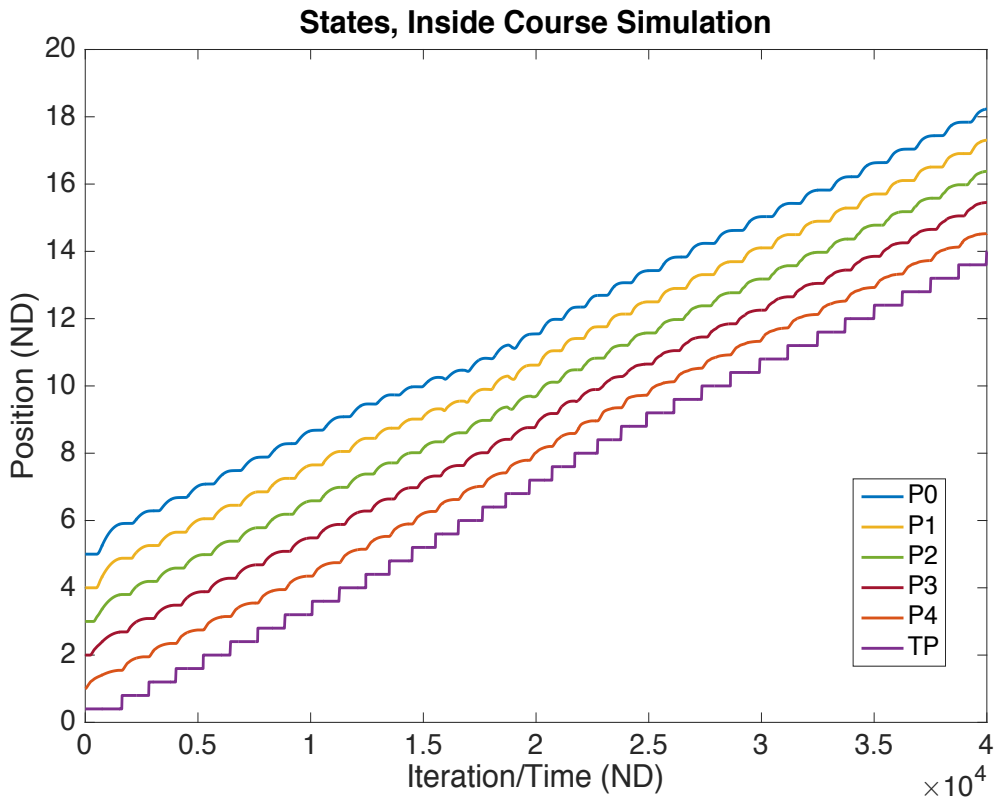

Figure 26 States during a simulation on the inside case where the radius of curvature is less than the minimum ($r<r_{min}$). In this case, there is a period of time where not all the crochets can engage.

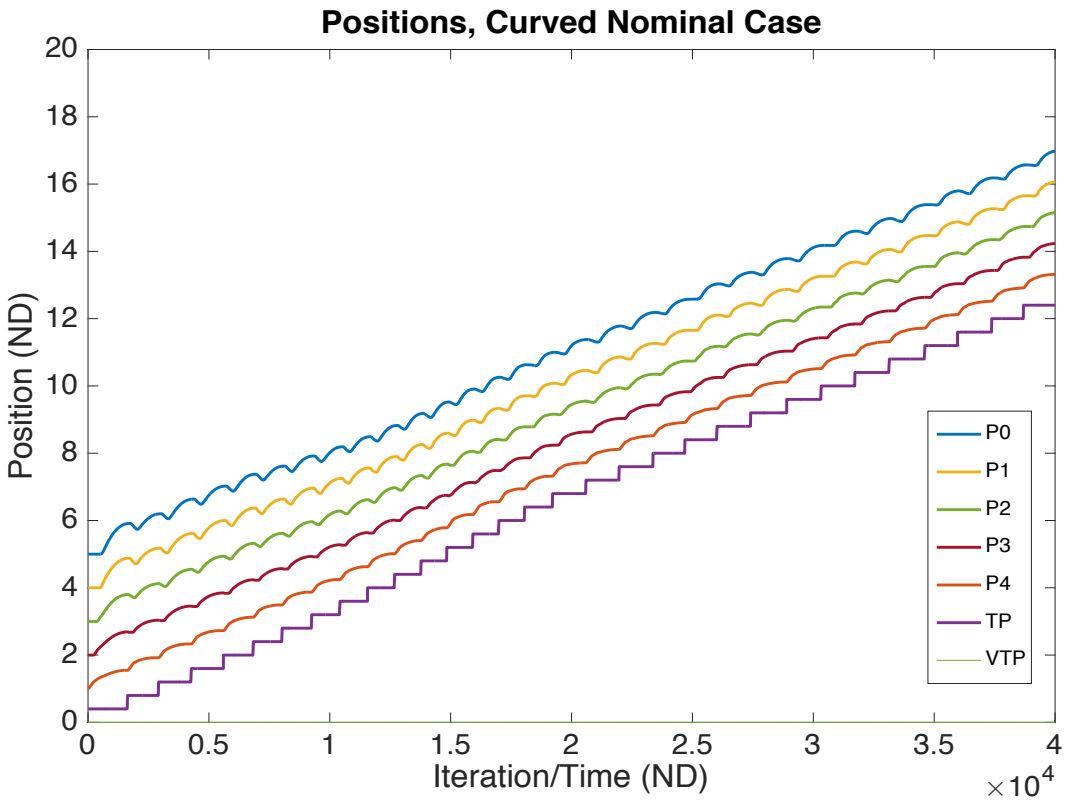

Figure 27 Comparison case where radius of curvature=r_{min}.

Figure 28 shows the crochet engagement through the simulation. Towards the left side of the plot, a sequence of crochet engagement similar to prior simulations is seen. As τ approaches 15000, we can see gait cycles where the first crochet doesn't engage. Over the next three gait cycles, only the last three crochets engage. Over the next two cycles, only two and then one crochet engages respectively. In the next cycle, the first crochet reengages again, as A_3 reaches the vertical surface. A few cycles later, the final crochet enters the fillet and ceases locking. By τ=27,500, all crochets are locking and unlocking each gait cycle. There are two key takeaways from this plot. The first is that, when the appropriate crochets are engaged, the anterograde wave prescribed by Schuldt is preserved. The second, is that the simulation successfully showed traversing the fillet with some, but not all, crochets unable to engage.

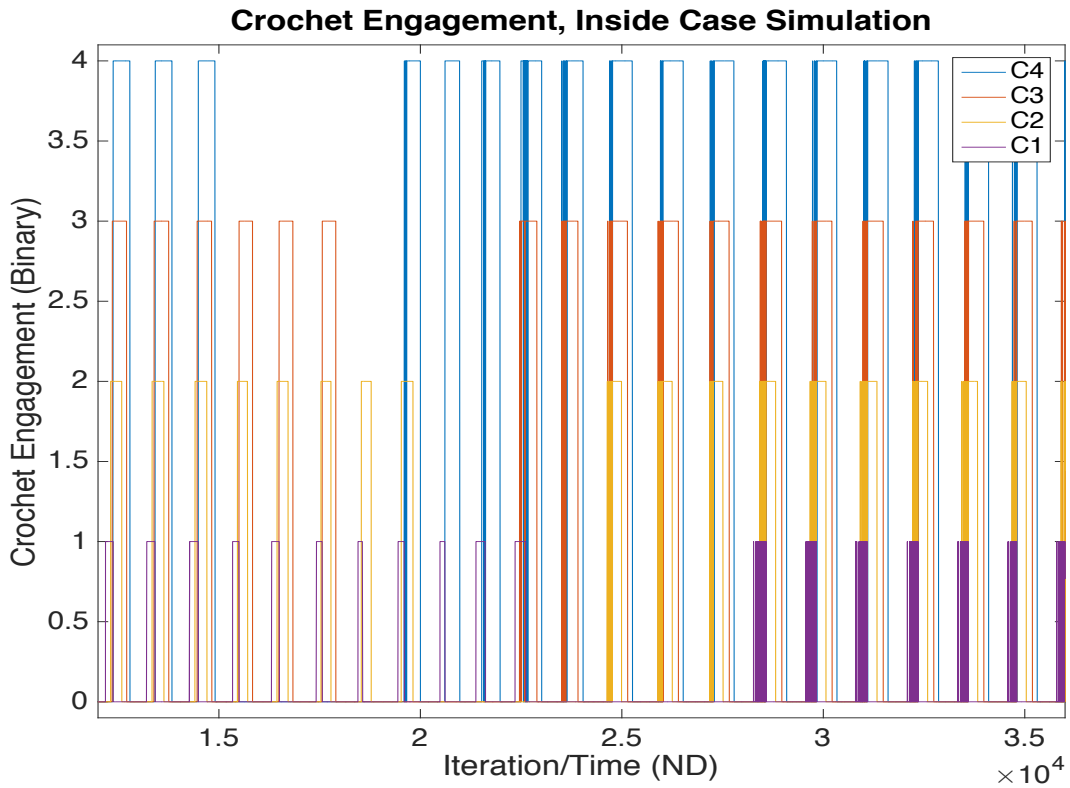

Figure 28 Crochet engagement during the portion of the simulation where crochets are not all crochets are able to engage.

Muscle engagement (Figure 29), shows increased chatter, but is otherwise unaffected by traversing the alternative course. This supports the success of the simulation; given that muscle activation is purely based on segment position, and not on any other factors (such as whether the crawler is on the substrate), its continued activation through the fillet helps confirm successful gait.

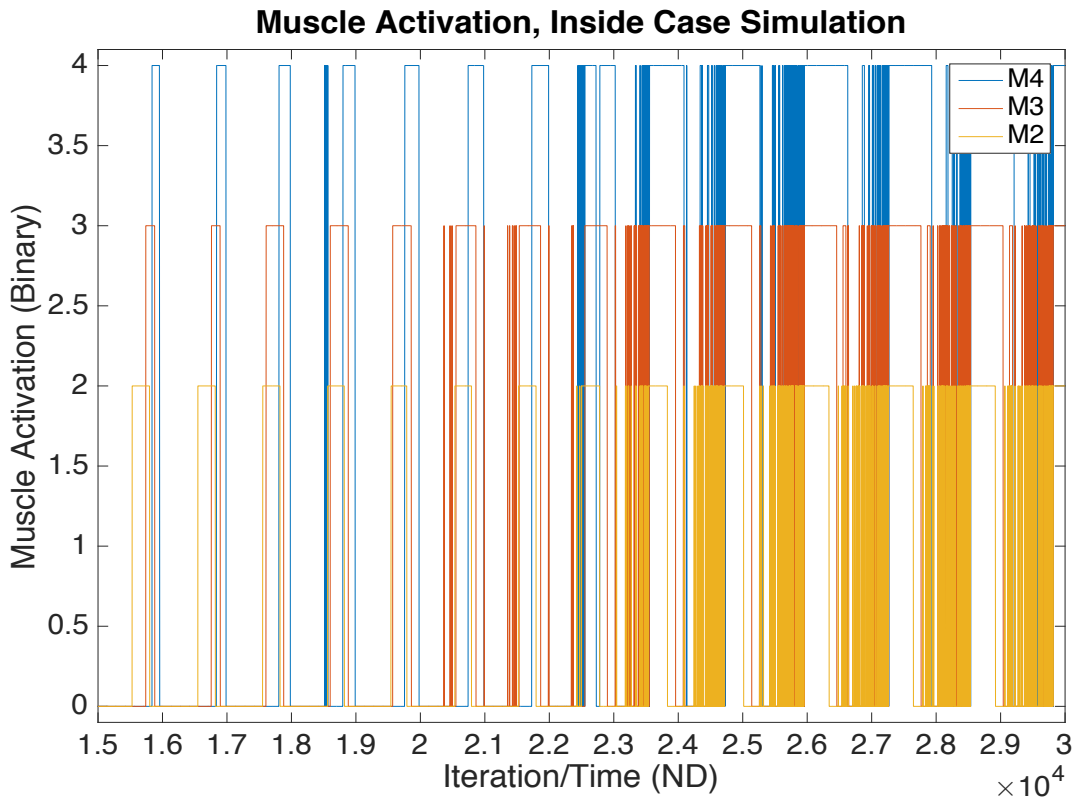

Figure 29 Crochet engagement through the inside case simulation.

Segment-specific gravity for the period while the crawler is on the fillet is shown in Figure 30. Effective gravity increases in a similar manner to the prior curved simulation, but with one exception. This exception is that, some decreases in segment-specific gravity are seen. Since the segments can now move freely with no crochet engagement on the alternative course, it is reasonable that there will be some backwards activity, and, with it, some decrease in effective gravity. Therefore, by applying previously discussed standards to these plots, gait on the inside case, even when the crochets can't engage for a certain portion of the simulation, is accomplishable and robust.

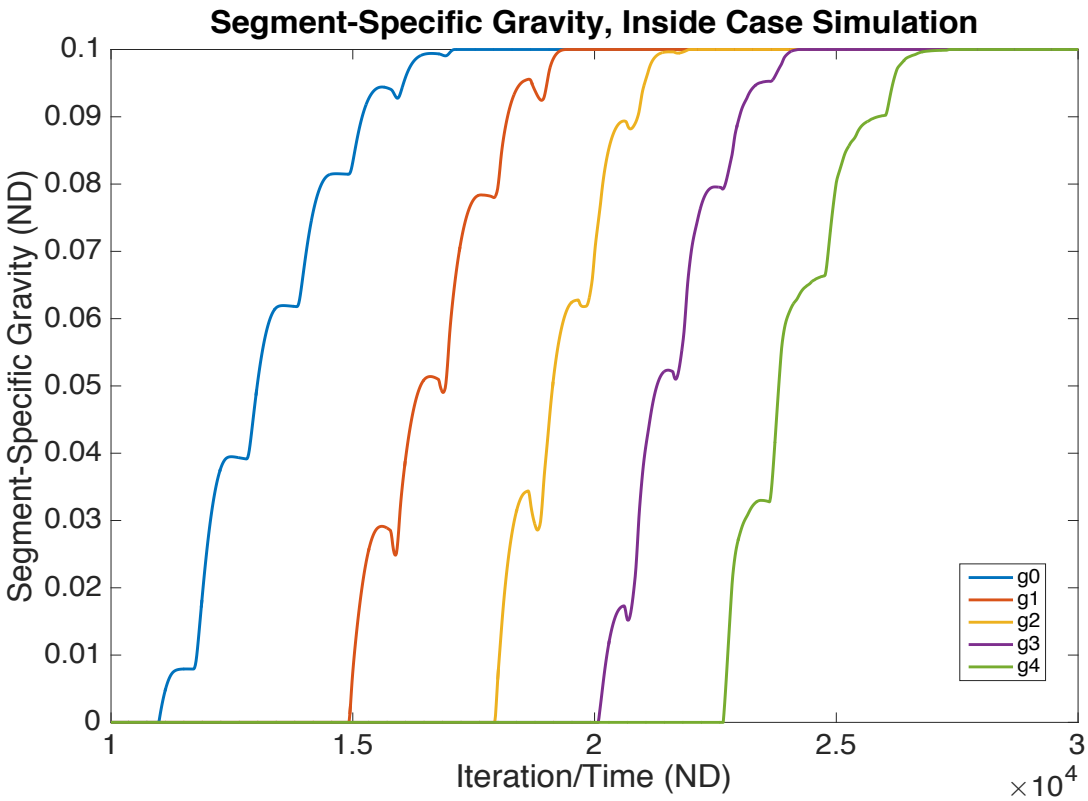

Figure 30 Segment-specific gravity throughout the inside case simulation.

iii. The Outside Case-Model

The outside case requires a decidedly different alternative course to tackle the $r<r_{min}$ scenario. Referencing Figure 31, the caterpillar proceeds normally along segment AB. After reaching the curve, it curls in the negative Z direction (with +Z out of the page). It's important to note that a The crawler follows this curvature for 180°, at which point it then curls in the positive Z direction to rejoin the substrate at point D. Along the alternative course, g_i is defined by the following piecewise function:

$$g_i = \begin{cases} 0 & x_i \leq L \\ g_{max} * \sin\frac{x-L+r_{min}}{r_{min}} & L < x_i \leq L + \frac{\pi}{2} r_{min} \\ g_{max} * \sin\frac{x-L+r_{min}-\frac{\pi * r_{min}}{2}}{r_{min}} & L + \frac{\pi}{2} r_{min} < x_i \leq L + \pi r_{min} \\ g_{max} * \sin\frac{x-L+(1-\pi)*r_{min}}{r_{min}} & L + \pi r_{min} < x_i \leq L + \frac{3\pi}{2} r_{min} \\ g_{max} & L + \frac{3\pi}{2} r_{min} < x_i \end{cases} \quad (25)$$

where L is the length from point A through the start of the circular portion of the alternative course. Factoring in the straight portion between point B and the start of the curve (length equal to r_{min}), the alternative course is equal to $\frac{5\pi r_{min}}{2}$.

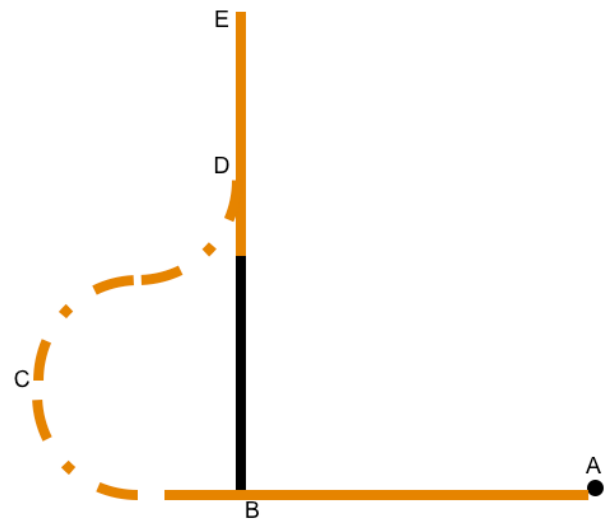

Figure 31 Alternative course for the outside case.

iv. Outside Case-Validation

The positional states resulting from a simulation of the outside case are shown in figure 32. The longer, more complex course necessitates more gait cycles and the resulting busier plot. That being said, a regular, controlled, repeatable gait is till visible. Some compression in overall length of the crawler (as denoted by the distance between the top and bottom curves) as well as some irregularity in the gait is visible in the region where the crawler is on the alternative course (τ>20000). Otherwise, the plots indicate a similar gait to what was seen in previous simulations.

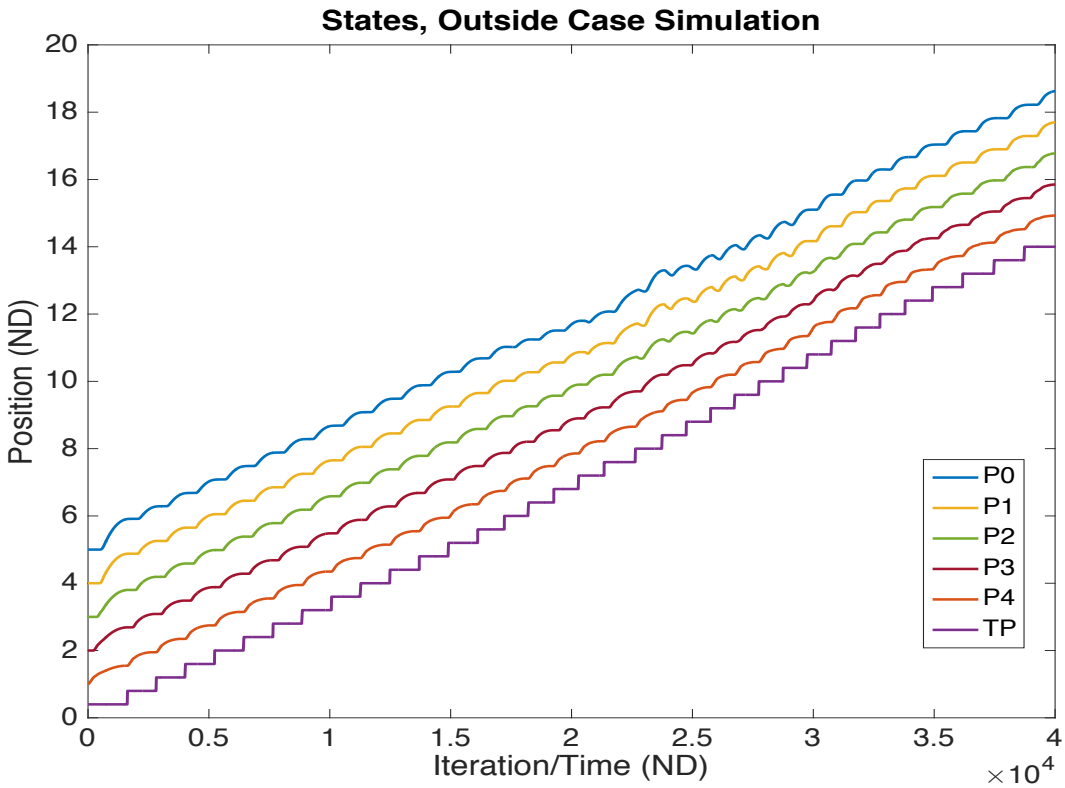

Figure 32 States during the outside case simulation.

In figure 33, crochet activation is seen through the outside case simulation. Much like in the inside case, regular cycles are observed, followed by the loss of engagement of the forward gripper. The next crochets follow, working toward the back. As the last gripper reaches the alternative course and loses its ability to engage, the first reaches the vertical surface. One by one, the grippers regain their ability to engage as the rest of the crawler's segments reach the vertical surface.

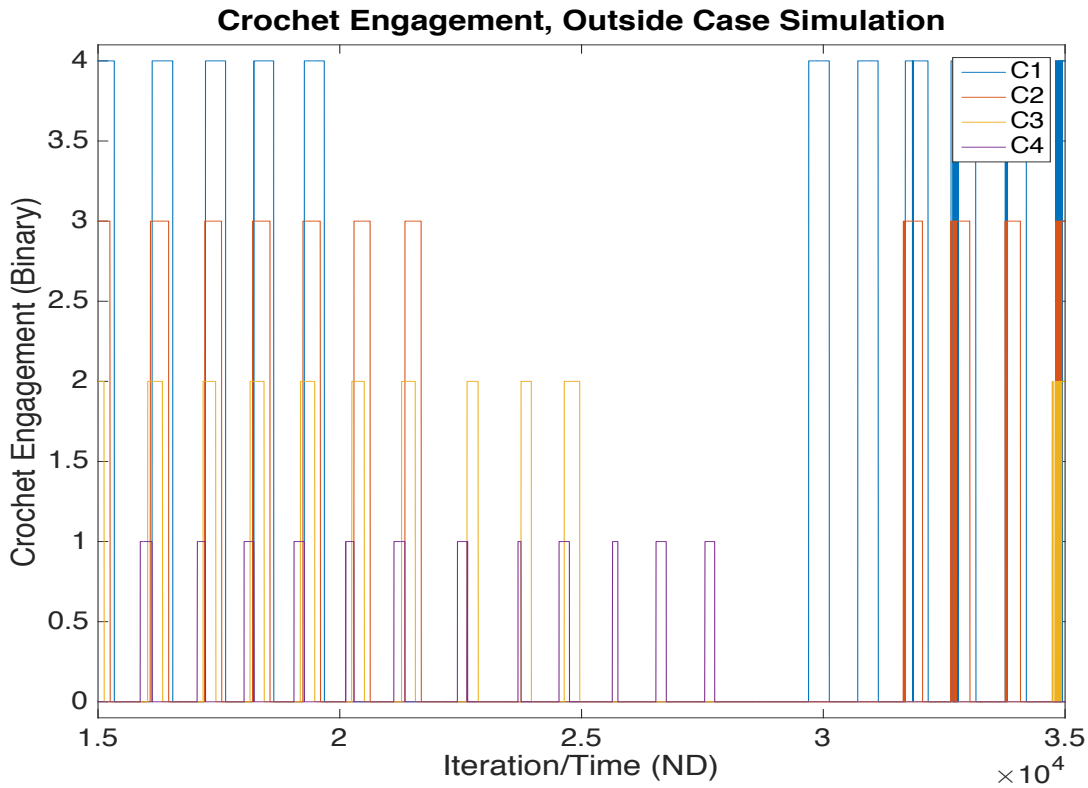

Figure 33 Crochet engagement while navigating the alternative course. Binary variables are multiplied by a constant for visual clarity.

Figure 34 shows muscle activation through the simulation, zoomed in on the portion where the crawler is on the alternative course. As has been seem previously, muscle activation is regular entering the alternative course. Increased chatter is seen through the inside course, with some irregularities as changing conditions are met. Finally, the crawler exits the course with more regular, albeit chatter-prone, activation.

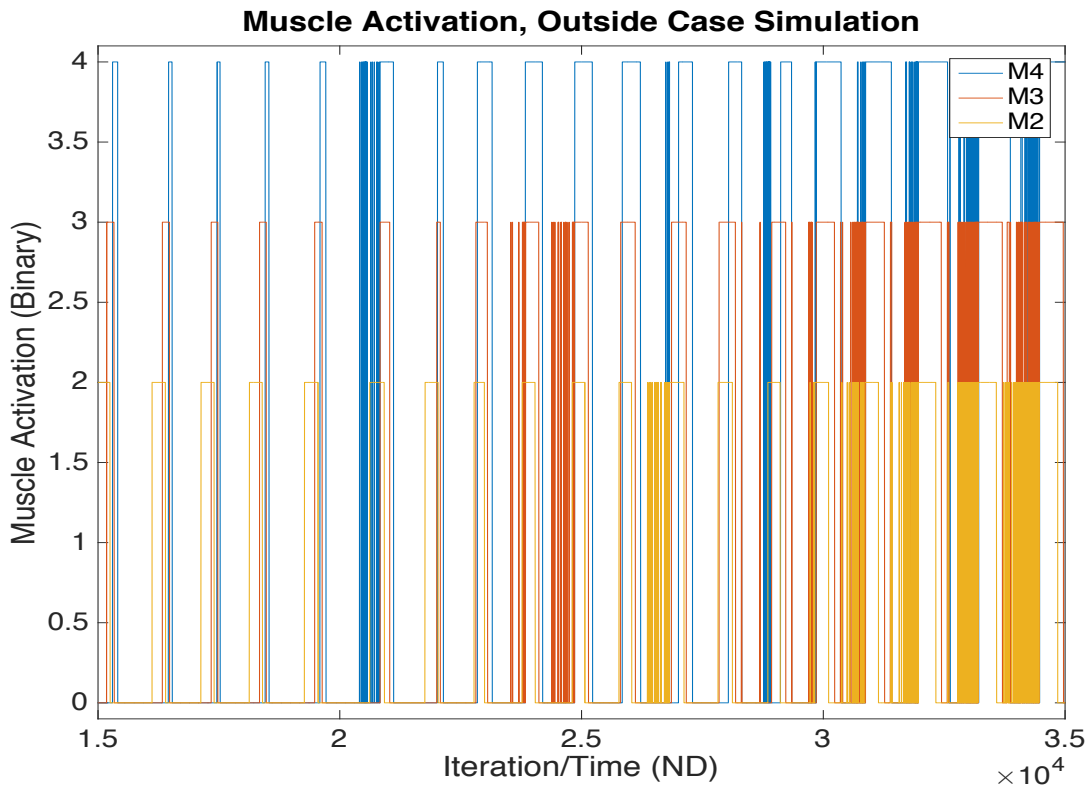

Figure 34 Muscle activation while navigating the outside course. Binary variables are multiplied by a constant for visual clarity.

Segment-specific gravity is shown in figure 35. Unlike the prior simulations in this chapter, segment-specific gravity in this simulation increases to g_{max}, decreases back to 0, and then returns to g_{max} while on the alternative course. Here, it is apparent that each segment encounters this in a similar pattern, as evidenced by each curve having similar geometry.

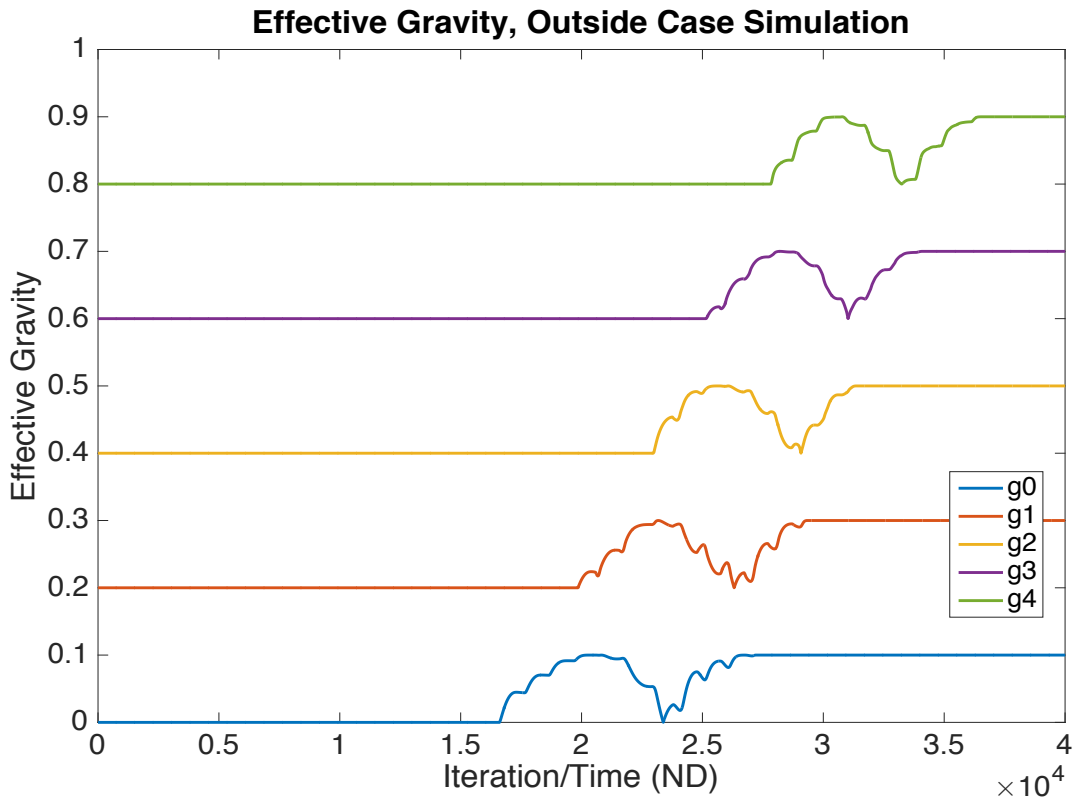

Figure 35 Effective gravity. Curves are displaced vertically by a constant for visual clarity.

Once again, robust gait is seen through evenly progressing gait cycles, anterograde crochet engagement and muscle activation, and repeatable gravitational loading. In both the inside and outside cases, the range of g_{max} mimicked that of g in the planar case. Figure 36 compares the ranges found.

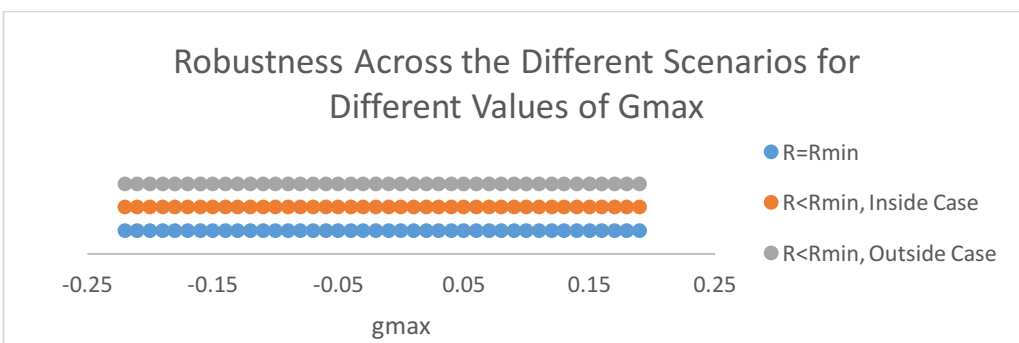

Figure 36 Comparison of ranges of Gmax for the different scenarios.

These two cases represent the final piece in applying Schuldt's model to a curved surface, particularly when that curved surface represents the transition zone between two other surfaces. For the model to be robust in this scenario, it needs to be adaptable to a gait cycle that doesn't involve all of the crochets. Through these simulations, that has been demonstrated.

4. Conclusion

A. Review of Contributions

This paper aims to demonstrate the robustness of the robustness of Schuldt's model for a caterpillar-like soft-body robot with reflex-based, local sensing control for travel over curved terrain. This is motivated by the notion that curved terrain can be an adequate surrogate for the transition zone between uneven planar terrain and because real-life terrain isn't always planar. To demonstrate robustness, a computer simulation was developed to model the behavior of the robot. As stated in the introduction, this thesis proposed the following two contributions:

1. Proposed that crawling on non-planar terrain can be modelled one-dimensionally by accounting for changing gravity and body distortion from curling.
2. Demonstrated, utilizing this non-planar model, that reflex-based crawling can be robust on a wide array of non-planar terrain.

After describing Schuldt's model and its limitations with regards to non-planar terrain, a modified version of the model was introduced in chapter 3. The simulation of gait over curved terrain is modeled with respect to two key factors: gravity and substrate geometry. While the prior work assumes all body segments face the same gravitational load, the loop solver successfully simulated gait under the varied gravitational load a robot would experience traversing a curved surface. However, when the curved surface begins to resemble a corner, the crawler must adapt by traveling a course that doesn't follow the substrate (with its crochets unable to reengage during this time). Two models were proposed (one for a convex curve and

the other for a concave curve) to explore the ability of the crawler to traverse the corners. Once again, successful gait was simulated.

B. Future Work

While this paper presents evidence that a caterpillar-like soft-bodied robot can successfully navigate a number of non-planar environments, to say the number of scenarios presented here is exhaustive would be a falsehood. With this in mind, future work could further examine possible environmental scenarios. However, it would likely be necessary to adapt the model presented by Schuldt and modified here to more accurately reflect two-dimensional motion. While the model has served its purpose well to this point, it has likely been taken as far as it can go.

Towards the goal of a more accurate model, future work should investigate a specific sensing suite. This will increase simulation fidelity in a couple of useful ways. Primarily, it will allow for greater accuracy in the type of data available to the muscle and crochet controllers. Additionally, it will further constrain the size, weight, and shape of the body segments, which have been largely approximated in this thesis. Another set of considerations of Jumbo importance that need to be explored are turning and navigation. Future work will need to examine the feasibility of including navigation hardware and the actuation to turn left or right relative to the substrate. All of this will ultimately lead to a more accurate simulation, with will hopefully inform the construction of a robust prototype (and then “mass-produced” version) to follow.

Key to development of a real-life crawler will be development of grippers to fill the role of crochets. The crochets serve as a prime motivation for modelling the crawler after a robot

due to their passive control and low-energy attachment mechanism. Transferring these advantages over to a mechanical crawler will be critical. Trimmer et. al. demonstrated the viability of utilizing a retractable silicone-based gripping pad for this purpose.[31] Their research showed that the pad could instantaneous apply <100 mN of localized traction (which is more than 5x higher than required force that has been found experimentally[32]). Other work has investigated the use of granular material that flows around and grips a substrate.[33] Future work could explore applying such attachment techniques to the model presented here.

C. Broader Impact

It is intended that this thesis will fit into a broader stream of work advancing soft-bodied robotics. Here, the modified model demonstrated robustness over a wide array of system and environmental parameters. With this work, the body of evidence supporting reflex-based crawling has been expanded. Robotics engineers interested in further developing soft-bodied systems now have an additional tool to utilize. Of course, the control law is only one component of a robotics system. Combined with novel grippers, new materials, and innovative manufacturing techniques, the possibilities are numerous. One day, a reflex-based crawler could be searching a disaster zone for survivors, or being used for less-invasive in-vivo diagnostics or interventions. It is the hope of the author that this thesis has contributed toward these goals, both for the better of humanity, and for science.

Appendix A-Code

i. Loop Solver

```
%Timing
t0=0;
int=.005;
tfinal=1200;
n=tfinal/int;

%Gait Cycle initializations
v=0;
vf=45;
ct=1000;
cl=ct;

%Data Collection
z=zeros(n,12);
y=zeros(n,4);
h=zeros(n,4);
j=zeros(n,4);
x=zeros(n,1);
s=zeros(vf,7);
u=zeros(n,5);

%System Parameters
lbar=1;
DR=1.5;
Apos=0.7;
Avel=0.012;
Aacc=0.2;
xbar=0.4;
g=0.1;
p=40; %non-dimensional curvature, which is referenced as the equivalent
radius of curvature in the text
rminimum=0.7;
con=2;%1 convex, 2 concave

%System initilaization
i=0;
q=zeros(12, 1);
r=[1 1 1 1 DR lbar 0 0 0 0 0];
q0=[5*lbar 0 4*lbar 0 3*lbar 0 2*lbar 0 lbar 0 xbar 0];

%Laplacian initializations
A=0;
B=0;
C=0;
D=0;
V1=0;
V2=0;
V3=0;
V4=0;
CrocOn=[0 0 0 0];

for t=t0:int:tfinal
```

```
    tf=t+int;
    i=i+1;
    x(i)=i;
    [t, q]=ode45(@(t,q) FiveSegmentTrailerPassColNDVaryGMinR(t,q,r), [t; tf],
q0);
    q0=q(end,:);
    z(i,:)=q(end,:);
    y(i,:)=[4*r(1) 3*r(2) 2*r(3) r(4)];
    %Distance Laplacian/Muscle Activation
    A=(-q0(1)+2*q0(3)-q0(5));
    B=(-q0(3)+2*q0(5)-q0(7));
    C=(-q0(5)+2*q0(7)-q0(9));
    D=(-q0(7)+2*q0(9)-q0(11));
    PhiA=((-q0(1)+2*q0(3)-q0(5))<0);
    PhiB=((-q0(3)+2*q0(5)-q0(7))<0);
    PhiC=((-q0(5)+2*q0(7)-q0(9))<0);
    PhiD=((-q0(7)+2*q0(9)-q0(11))<0);
    PhiE=0;
    %Velocity Laplacian
    V1=-q0(2)+2*q0(4)-q0(6);
    V2=-q0(4)+2*q0(6)-q0(8);
    V3=-q0(6)+2*q0(8)-q0(10);
    V4=-q0(8)+2*q0(10)-q0(12);
    %Data Logging
    h(i,:)=[4*PhiA 3*PhiB 2*PhiC PhiD];
    j(i,:)=[A 2*B 3*C 4*D];
    u(i,:)=[r(7) r(8) r(9) r(10) r(11)];
    if r(1)==0
        if (((q0(1)-q0(5))>Apos) & (abs(q0(4))<Avel) & ((-2*DR*V1-A+(PhiA-
PhiB)-r(8))<Aacc))& (CrocOn(1)==0)
            r(1)=1;
        end
    elseif r(1)==1
        if (-A+(PhiA-PhiB)-r(8))>(Aacc)
            r(1)=0;
        end
    end
    if r(2)==0
        if (((q0(3)-q0(7))>Apos) & (abs(q0(6))<Avel) & ((-2*DR*V2-B+(PhiB-
PhiC)-r(9))<Aacc)) &(CrocOn(2)==0)
            r(2)=1;
        end
    elseif r(2)==1
        if (-B+(PhiB-PhiC)-r(9))>Aacc
            r(2)=0;
        end
    end
    if r(3)==0
        if (((q0(5)-q0(9))>Apos) & (abs(q0(8))<Avel) & ((-2*DR*V3-C+(PhiC-
PhiD)-r(10))<Aacc))&(CrocOn(3)==0)
            r(3)=1;
        end
    elseif r(3)==1
        if (-C+(PhiC-PhiD)-r(10))>Aacc
            r(3)=0;
        end
    end
    if r(4)==0
```

```
        if (((q0(7)-q0(11))>Apos) & (abs(q0(10))<Avel) & ((-2*DR*V4-D+(PhiD-
PhiE)-r(11))<Aacc))&(CrocOn(4)==0)
            r(4)=1;
        end
    elseif r(4)==1 %will this be triggered by changing r(4)?
        if (-D+(PhiD-PhiE)-r(11))>Aacc
            r(4)=0;
        end
    end
Vec1=CourseMinR(q0(1), g, lbar, p, rminimum, con);
        r(7)=Vec1(1);
        Vec2=CourseMinR(q0(3), g, lbar, p, rminimum, con);
        r(8)=Vec2(1);
        CrocOn(1)=Vec2(2);
        Vec3=CourseMinR(q0(5), g, lbar, p, rminimum, con);
        r(9)=Vec3(1);
        CrocOn(2)=Vec3(2);
        Vec4=CourseMinR(q0(7), g, lbar, p, rminimum, con);
        r(10)=Vec4(1);
        CrocOn(3)=Vec4(2);
        Vec5=CourseMinR(q0(9), g, lbar, p, rminimum, con);
        r(11)=Vec5(1);
        CrocOn(4)=Vec5(2);
    if i>cl & (r(1)==1|CrocOn(1)==1) & (r(2)==1|CrocOn(2)==1) &
(r(3)==1|CrocOn(3)==1) & (r(4)==1|CrocOn(4)==1)
        if v<vf
            v=v+1;
            s(v, 1)=q0(1);
            s(v, 2)=q0(3);
            s(v, 3)=q0(5);
            s(v, 4)=q0(7);
            s(v, 5)=q0(9);
            s(v, 6)=q0(11);
            q0(11)=q0(11)+0.4;
            cl=i+ct;
        end
    end
end
```

ii. ODE Function File

```
function qdot=FiveSegmentTrailer(t, q, r)
DR=r(5);
lbar=r(6);
g0=r(7);
g1=r(8);
g2=r(9);
g3=r(10);
g4=r(11);

%Muscles
A=((-q(1)+2*q(3)-q(5))<0);
B=((-q(3)+2*q(5)-q(7))<0);
C=((-q(5)+2*q(7)-q(9))<0);
D=((-q(7)+2*q(9)-q(11))<0);
E=0;

%Distance Laplacian
```

```
DL1=-q(1)+2*q(3)-q(5);
DL2=-q(3)+2*q(5)-q(7);
DL3=-q(5)+2*q(7)-q(9);
DL4=-q(7)+2*q(9)-q(11);

%Velocity Laplacian
VL1=-q(2)+2*q(4)-q(6);
VL2=-q(4)+2*q(6)-q(8);
VL3=-q(6)+2*q(8)-q(10);
VL4=-q(8)+2*q(10)-q(12);

xdot1=q(2);
vdot1=(2*DR*(q(4)-q(2)))-(q(1)-q(3)-lbar)-g0;
if r(1)==0
    xdot2=q(4);
vdot2=-2*DR*VL1-DL1+(A-B)-g1;
elseif r(1)==1
    xdot2=0;
    vdot2=0;
end
if r(2)==0
    xdot3=q(6);
    vdot3=-2*DR*VL2-DL2+(B-C)-g2;
elseif r(2)==1
    xdot3=0;
    vdot3=0;
end
if r(3)==0
    xdot4=q(8);
    vdot4=-2*DR*VL3-DL3+(C-D)-g3;
elseif r(3)==1
    xdot4=0;
    vdot4=0;
    end
if r(4)==0
    xdot5=q(10);
    vdot5=-2*DR*VL4-DL4+(D-E)-g4;
elseif r(4)==1
    xdot5=0;
    vdot5=0;
end
xdot6=0;
vdot6=0;
qdot=[xdot1; vdot1; xdot2; vdot2; xdot3; vdot3; xdot4; vdot4; xdot5; vdot5;
xdot6; vdot6];
end
```

iii. Course File

```
function vec=CourseMinR(x, g, l, ratio, min, type)
radius=6*l/ratio; %ratio is the non-dimensional curvature
rmin=min;
off=0;
if radius>=rmin
    if x<=10*l
        Gout=0;
    elseif x>10*l & x<((10*l)+(pi*radius/2))
         Gout=g*sin((x-(10*l))/radius);
```

```
    else
        Gout=g;
    end
elseif type==1 %convex
    if x<=10*l+rmin
        Gout=0;
    elseif x>10*l+rmin & x<((10*l)+rmin+(pi*rmin/2))
         Gout=g*sin((x-((10*l)+rmin))/rmin);
         off=1;
    elseif x>((10*l)+rmin+(pi*rmin/2)) & x<((10*l)+rmin+(pi*rmin))
         Gout=g*sin((x-((10*l)-rmin)-(pi*rmin/2))/rmin);
         off=1;
    elseif x>((10*l)+rmin+(pi*rmin)) & x<((10*l)+rmin+(3*pi*rmin/2))
         Gout=g*sin((x-((10*l)+rmin)-(pi*rmin))/rmin);
         off=1;
    else
        Gout=g;
    end
else %type=2 Concave
    if x<=10*l-rmin
        Gout=0;
    elseif x>10*l-rmin & x<((10*l)-rmin+(pi*rmin/2))
         Gout=g*sin((x-((10*l)-rmin))/rmin);
         off=1;
    else
        Gout=g;
    end
end
    vec=[Gout; off]; %Gout is segment specific gravity.  Off determines
whether the crochet is disengaged.
end
```

REFERENCES

1. Rus, Daniela, and Michael T. Tolley. "Design, fabrication and control of soft robots." *Nature* 521.7553 (2015): 467-75. Web.

2. Lohsiriwat, Varut. "Colonoscopic perforation: Incidence, risk factors, management and outcome." *World Journal of Gastroenterology* 16.4 (2010): 425-30.

3. Polygerinos, Panagiotis, Zheng Wang, Kevin C. Galloway, Robert J. Wood, and Conor J. Walsh. "Soft robotic glove for combined assistance and at-home rehabilitation." *Robotics and Autonomous Systems* 73 (2015): 135-43. Web.

4. Jung, Kwangmok, Ja Choon Koo, Jae-Do Nam, Young Kwan Lee, and Hyouk Ryeol Choi. "Artificial annelid robot driven by soft actuators." *Bioinspiration & Biomimetics* 2.2 (2007): S42-49

5. Seok, Sangok, Cagdas Denizel Onal, Kyu-Jin Cho, Robert J. Wood, Daniela Rus, and Sangbae Kim. "Meshworm: A Peristaltic Soft Robot With Antagonistic Nickel Titanium Coil Actuators." *IEEE/ASME Transactions on Mechatronics* 18.5 (2013): 1485-497.

6. Laschi, Cecilia, Matteo Cianchetti, Barbara Mazzolai, Laura Margheri, Maurizio Follador, and Paolo Dario. "Soft Robot Arm Inspired by the Octopus." *Advanced Robotics* 26.7 (2012): 709-27.

7. Mazzolai, B., L. Margheri, M. Cianchetti, P. Dario, and C. Laschi. "Soft-robotic arm inspired by the octopus: II. From artificial requirements to innovative technological solutions." *Bioinspiration & Biomimetics* 7.2 (2012): 025005.

8. Marchese, Andrew D., Cagdas D. Onal, and Daniela Rus. "Autonomous Soft Robotic Fish Capable of Escape Maneuvers Using Fluidic Elastomer Actuators." *Soft Robotics* 1.1 (2014): 75-87.

9. Onal, Cagdas. D., Chen, Xin, Whitesides, George M. & Rus, Daniela. Soft mobile robots with on-board chemical pressure generation. In Proc. International Symposium on Robotics Research 1-16 (2011).

10. Lin, Huai-Ti, Gary G. Leisk, and Barry Trimmer. "GoQBot: a caterpillar-inspired soft-bodied rolling robot." *Bioinspiration & Biomimetics* 6.2 (2011): 026007. Web.

11. Tolley, Michael T., Robert F. Shepherd, Bobak Mosadegh, Kevin C. Galloway, Michael Wehner, Michael Karpelson, Robert J. Wood, and George M. Whitesides. "A Resilient, Untethered Soft Robot." *Soft Robotics* 1.3 (2014): 213-23.

12. Onal, Cagdas D., and Daniela Rus. "Autonomous undulatory serpentine locomotion utilizing body dynamics of a fluidic soft robot." *Bioinspiration & Biomimetics* 8.2 (2013): 026003.

13. Shepherd, Robert F., Adam A. Stokes, Jacob Freake, Jabulani Barber, Phillip W. Snyder, Aaron D. Mazzeo, Ludovico Cademartiri, Stephen A. Morin, and George M. Whitesides. "Using Explosions to Power a Soft Robot." *Angewandte Chemie* 125.10 (2013): 2964-968. Web.

14. Schuldt, Dieter W., Jason Rife, and Barry Trimmer. "Template for robust soft-body crawling with reflex-triggered gripping." *Bioinspiration & Biomimetics* 10.1 (2015): 016018.

15. Van Griethuijsen, Linnea I.N.N. "Behavioral Responses to Mechano-Sensory Information in a Soft-Bodied Terrestrial Animal." Diss. Tufts U, 2012. Abstract. (n.d.): n. pag. Print.

16. van Griethuijsen, L. I., and B. A. Trimmer. "Locomotion in caterpillars." *Biological Reviews* 89.3 (2014): 656-70. Web.

17. Lin, H.-T., D. J. Slate, C. R. Paetsch, A. L. Dorfmann, and B. A. Trimmer. "Scaling of caterpillar body properties and its biomechanical implications for the use of a hydrostatic skeleton." *Journal of Experimental Biology* 214.7 (2011): 1194-204. Web.

18 Saunders, Frank, Barry A. Trimmer, and Jason Rife. "Modeling locomotion of a soft-bodied arthropod using inverse dynamics." *Bioinspiration & Biomimetics* 6.1 (2010): 016001. Web.

19. Barbier, R. 1985. “Morphogenèse et evolution de la cuticule et des crochets des fausses-pattes, au cours du développement larvaire de Galleria mellonella L.(Lepidoptera, Pyralidae).” Bull. Soc. Zoologique France 110 205–21

20. Belanger, Jim H., and Barry A. Trimmer. "Combined kinematic and electromyographic analyses of proleg function during crawling by the caterpillar Manduca sexta." *Journal of Comparative Physiology A: Sensory, Neural, and Behavioral Physiology* 186.11 (2000): 1031-039.

21. Chen, Li, Shugen Ma, Yuechao Wang, Bin Li, and Dengping Duan. "Design and modelling of a snake robot in traveling wave locomotion." *Mechanism and Machine Theory* 42.12 (2007): 1632-642. Web.

22. Date, Hisashi, and Yoshihiro Takita. "Adaptive Locomotion of a Snake Like Robot Based on Curvature Derivatives." Proceedings of the 2007 IEEE/RSJ International Conference on Intelligent Robots and Systems, 2007: 3554-3559.

23. "Caterpillar crawling on leaf public domain free photos for download." *ABSFreePic.com*. N.p., n.d. Web. 23 Apr. 2017. <http://absfreepic.com/free-photos/download/caterpillar-crawling-on-leaf-3505x2336_26486.html>.

24. "Big caterpillar on tree." *ABSFreePic.com*. N.p., n.d. Web. 28 Apr. 2017. <http://absfreepic.com/free-photos/download/big-caterpillar-on-tree-3648x2736_81198.html>.

25 Morse, Paul. "911: Ground Zero." *National Archives and Records Administration*. National Archives and Records Administration, n.d. Web. 28 Apr. 2017.

26. *Wikimedia Commons*. The Wikimedia Foundation, n.d. Web. 10 Apr. 2017. <https://commons.wikimedia.org/wiki/File:Diagram_showing_a_colonoscopy_CRUK_060.svg>.

27. *Wikimedia Commons*. The Wikimedia Foundation, n.d. Web. 1 May 2017. < https://commons.wikimedia.org/wiki/File:Monarch_caterpillar_on_swan_plant_branchlet.jpg>.

28. Matlab R2015, The Mathworks, Inc., Natick, Massachusetts.

29. Daltorio, Kathryn A., Timothy C. Witushynsky, Gregory D. Wile, Luther R. Palmer, Anas Ab Malek, Mohd Rasyid Ahmad, Lori Southard, Stanislav N. Gorb, Roy E. Ritzmann, and Roger D. Quinn. "A body joint improves vertical to horizontal transitions of a wall-climbing robot." *2008 IEEE International Conference on Robotics and Automation* (19-23 May 2008): n. pag. *Semantic Scholar*. Web. 7 May 2017.

30. Park, Jongwon, Young Kook Kim, Won Suk Jung, Kyung-Soo Kim, and Soohyun Kim. "Ground following locomotion of a robot inspired by pill bugs." *2011 IEEE International Conference on Robotics and Biomimetics* (12 April 2012): n. pag. *IEEE Explore*. Web. 7 May 2017.

31. Trimmer, Bary A., Huai-Ti Lin, Amanda Baryshyan, Gary G. Leisk, and David L. Kaplan. "Towards a biomorphic soft robot: Design constraints and solutions." *IEEE Xplore*. Proc. of Biomedical Robotics and Biomechatronics (BioRob), 2012 4th IEEE RAS & EMBS International Conference on, Rome. IEEE, 31 Aug. 2012. Web. 7 May 2017.

32. Lin, H.-T., and B. A. Trimmer. "The substrate as a skeleton: ground reaction forces from a soft-bodied legged animal." *Journal of Experimental Biology* 214.14 (2011): 2451. Web.

33. Amend, John R., Eric Brown, Nicholas Rodenberg, Heinrich M. Jaeger, and Hod Lipson. "A Positive Pressure Universal Gripper Based on the Jamming of Granular Material." *IEEE Transactions on Robotics* 28.2 (2012): 341-50. Web.